

Identification and Functional Characterization of The Neuronal Pathway Regulating Insect Steroid Hormone Biosynthesis

A Dissertation Submitted to
the Graduate School of Life and Environmental Sciences,
the University of Tsukuba
in Partial Fulfillment of the Requirements
for the Degree of Doctor of Philosophy in Science
(Doctoral Program in Biological Sciences)

Eisuke IMURA

Table of contents

Abstract.....	2
Abbreviations	3
Introduction	5
Results	6
Discussion	12
Methods.....	15
Figures	20
Acknowledgements.....	43
References	44

Abstract

Steroid hormones are key players for many aspects of development, growth, and reproduction in multicellular organisms. In insects, the principal steroid hormones, ecdysteroids, coordinate growth and maturation. In *Drosophila*, a peak in ecdysteroid concentration triggers developmental transitions culminating with molting and metamorphosis. Moreover, recent studies shed light on the basal levels of ecdysteroids, which negatively affect body growth prior to maturation. Ecdysteroid biosynthesis in the prothoracic gland (PG) is affected by several signals, especially neuronal signals, and controls the proper timing of growth and maturation. The prothoracicotropic hormone (PTTH)-producing neurons and serotonergic $SE0_{PG}$ neurons innervate the PG, regulating ecdysteroid biosynthesis. However, only these two types of neurons may not account for the precise timing of basal and peak of ecdysteroid biosynthesis in response to the complex combination of environmental stimuli. Consequently, I hypothesized that other neuronal regulatory systems must exist in the PG. Based on this hypothesis, I aimed to identify and characterize novel PG-innervating neurons.

Using the FlyLight database, I found several types of PG-innervating neurons that have not yet been fully characterized. Among these neurons, I focused on three pairs of Corazonin (*Crz*)-producing neurons, which contact PTTH neurons and PG cells. Inhibition of *Crz* neuronal activity increased pupal size, whereas it had little effect on pupariation timing. This phenotype resulted from enhanced growth and a delay in basal ecdysteroid elevation during the mid-third instar larval (L3) stage. Silencing of *Crz* in *Crz* neurons resulted in increased levels of *bantam* microRNA, which represses basal ecdysteroid biosynthesis.

To examine whether PG cells receive *Crz*, I visualized the expression of *CrzR*. Unexpectedly, *CrzR* was expressed in PTTH neurons rather than PG cells. Silencing of *CrzR* in PTTH neurons exhibited increased pupal size, phenocopying the inhibition of *Crz* neurons. Interestingly, *Crz receptor (CrzR)* expression in PTTH neurons was higher during the mid-L3 stage than during the late-L3 stage. When *Crz* neurons were optogenetically activated, a strong calcium response was observed in PTTH neurons in the mid-, but not the late-L3 stage larvae brains. These data suggest that the *Crz*-PTTH neuronal axis modulates basal, but not peak ecdysteroid biosynthesis. Most significantly, this study uncovered a regulatory neuronal system affecting ecdysteroid biosynthesis in a developmental stage-specific manner.

Abbreviations

20E: 20-Hydroxyecdysone

AH: After Hatching

AstA: Allatostatin A

AstAR1: Allatostatin A Receptor 1

Ban: Bantam

CATMAID: Collaborative Annotation Toolkit for Massive Amounts of Image Data

Crz: Corazonin

CrzR: Corazonin Receptor

DCV: Dense Core Vesicle

Dilp: Drosophila Insulin-Like Peptide

ELISA: Enzyme-Linked Immunosorbent Assay

FSH: Follicle-Stimulating Hormone

GCaMP6s: GFP Based Ca²⁺ Calmodulin Probes

GnRH: Gonadotropin-Releasing Hormone

GnRHR: Gonadotropin-Releasing Hormone Receptor

GRASP: GFP Reconstitution Across Synaptic Partners

HPG axis: Hypothalamic-Pituitary-Gonadal Axis

IPC: Insulin-Producing Cell

KISS: Kisspeptin

KISSR: Kisspeptin Receptor

L1: 1st instar Larva

L3: 3rd instar Larva

LC-MS/MS: Liquid Chromatography/Mass Spectrometry

Lgr3: Leucine Rich Repeat Containing G protein Coupled Receptor 3

LH: Luteinizing Hormone

Oamb: Octopamine Receptor in Mushroom Bodies

PDF: Pigment-Dispersing Factor

PG: Prothoracic Gland

PTTH: Prothoracicotropic Hormone

RG: Ring Gland

SEZ: Subesophageal Zone

sNPF: Short Neuropeptide F

Sro: Shroud

TbH: Tyramine β Hydroxylase

Tdc2: Tyrosine Decarboxylase 2

TeTxLC: Tetanus Toxin Light Chain

Wts: Warts

Yki: Yorkie

Introduction

During development, many organisms undergo a maturation step to transition from infertile juvenile to fertile adult, similar to puberty in mammals. The onset of sexual maturation coincides with the end of the growth period. Therefore, a coordination of growth and sexual maturation is required to ensure appropriate adult size and fertility. One of the biomolecules that control growth and sexual maturation are steroid hormones. The timing of steroid hormone biosynthesis is controlled through a neuro-endocrine mechanism that acts at the level of biosynthetic organs. This neuro-endocrine mechanism regulates steroid hormone biosynthesis in response to environmental stimuli and ensures proper timing of sexual maturation [1–3].

The fruit fly *Drosophila melanogaster* is an excellent model organisms to study of the neuro-endocrine mechanism that controls steroid hormone biosynthesis. In insects such as *D. melanogaster*, the principal steroid hormones, ecdysteroids, coordinate juvenile growth and maturation, which includes molting and metamorphosis [4]. During larval stages, ecdysteroids are biosynthesized in the specialized endocrine organ known as the prothoracic gland (PG) (**Figure 1A**), and secreted into the hemolymph [5]. Ecdysteroids control the expression of various genes and their levels fluctuate depending on the developmental stage [6,7]. Previous studies showed that peaks in ecdysteroid levels trigger developmental transitions such as maturation, whereas basal levels negatively affect body growth, at least in part, by repressing insulin signaling [8–10]. In addition, recent studies showed that ecdysteroid biosynthesis is regulated through Warts (Wts)/Yorkie (Yki)/microRNA *bantam* (*ban*) signaling in the PG (**Figure 1B**) [11,12].

Ecdysteroid biosynthesis in the PG is affected by several environmental cues, such as photoperiod and nutrition [13,14]. Therefore, various mechanisms to regulate ecdysteroid biosynthesis must be put in place, and the neuronal regulatory mechanism may be essential for controlling the proper timing of growth and maturation in response to environmental cues (**Figure 1B**). So far, prothoracicotrophic hormone (PTTH)-producing neurons (PTTH neurons) and $SE0_{PG}$ serotonergic neurons have been shown to project to the PG and regulate ecdysteroid biosynthesis (**Figure 1A**) [15–17]. However, only these two types of neurons might not account for the precise timing of ecdysteroid biosynthesis in response to the complex combination of environmental stimuli. Indeed, other types of neurons involved in the regulation on ecdysteroid biosynthesis have been identified in *Bombyx mori*, *Mamestra brassicae*, and *Periplaneta americana* [18–21]. Given this situation, I hypothesized that other regulatory neuronal systems that regulate basal levels of ecdysteroid should exist in the PG. Based on this hypothesis, I aimed to identify and characterize novel PG-innervating neurons.

Results

Identification of PG-innervating Corazonin neurons using FlyLight database

To identify additional types of neurons innervating the PG, I screened the *Janelia* neuronal GAL4 collection to identify driver lines expressing GAL4 in neurons projecting toward the PG with FlyLight database (<https://www.janelia.org/project-team/flylight>) [22–24]. This database provides images from over 10000 GAL4 strains, in which different subsets of neurons are labeled using the GAL4/UAS system. Among them, I selected 79 GAL4 strains as candidates that exhibit labeled PG-innervating neurons. Next, I visualized these strains myself and confirmed their target sites. As a result, in addition to previously confirmed PG-innervating neurons, I have identified a novel candidate of PG-innervating neurons labeled by *R41A04-GAL4*. A FLP-out GAL4 clone using the *R41A04-GAL4* driver showed that single neurons clearly projected to the PG from one side of the brain hemisphere (**Figure 2A**) [25,26].

During anatomical analyses, I found that the position of the cell body of novel candidate PG-innervating neurons was similar to that of neurons producing the neuropeptide called Corazonin (Crz) [27]. The neuropeptide Crz is present in most major lineages of insects and has pleiotropic functions in various species [28]. These Crz neurons were originally reported to innervate the ring gland (RG), which is a composite endocrine organ composed of the PG, corpora allata, and corpora cardiaca [15,29]. Nonetheless, the function of RG-projecting Crz neurons has not been characterized yet. Consequently, I performed immunostaining with anti-Crz antibodies. Anti-Crz signal was observed in the novel candidate of PG-innervating neurons, both in the terminal axon projecting to the PG and the cell body (**Figure 2B**). Altogether, these data show that PG-innervating neurons are Crz neurons.

Crz neurons establish neuronal connections with PG cells

To examine whether Crz neurons establish synaptic contacts with PG cells, I conducted GFP Reconstitution Across Synaptic Partners (GRASP) analysis (**Figure 3A**) [20], in which two complementary fragments of GFP were expressed in Crz neurons and PG cells, respectively. GFP reconstruct signals appeared on the PG, suggesting that Crz neurons are located close enough to establish neuronal connections with PG cells (**Figure 3B**). However, in the GRASP assay, GFP would be reconstructed when the distance between cells is lower than 100 nm; consequently, positive signal does not always imply that Crz neurons establish neuronal connections with PG cells.

Given this limitation, to investigate the connections between Crz neurons and PG cells at the ultrastructural level, I conducted connectome analyses using the web-based Collaborative Annotation Toolkit for Massive Amounts of Image Data (CATMAID) in collaboration with Dr. Albert Cardona (*Janelia* Research Campus) and Dr. Michael Pankratz

(University of Bonn) [30,31]. CATMAID allowed us to reconstruct neurons and their presynaptic partners, providing a comprehensive anatomical view. The data set comprises an entire central nervous system and the RG of the first instar larval (L1) stage. A previous study reported that circuit connectivity properties remain largely unchanged throughout larval development in *D. melanogaster*, whereas neuronal arbor morphology and synapse number may change to some extent [32]. Neuropeptides are produced in cell bodies and packaged into dense core vesicles (DCVs) before being transported to their release sites [33]. It is conceivable that local swellings along the main neurites, which feature multiple presynaptic sites and DCVs, might enable local peptide release [34]. Hence, I marked DCV fusion sites with presynaptic density and DCVs on Crz neurons (**Figure 4A, B**). As a result, I detected DCV fusion sites between Crz neurons and PG cells (**Figure 4C**). Altogether, these data strongly supported that Crz neurons are connected to PG cells.

Crz neurons negatively control systemic body growth by regulating basal ecdysteroid biosynthesis

To explore the role of Crz in the regulation of ecdysteroid biosynthesis, I examined whether Crz neurons affect growth and maturation. Using the *Crz-GAL4* strain, in which three pairs of Crz neurons are predominantly labeled in the brain (**Figure 5A**) [35], I inhibited the activity of Crz neurons by expressing *kir2.1*, which encodes the inward-rectifier potassium ion channel [36,37]. Pupal body size was increased in *Crz>kir2.1* larvae compared to control (*Crz>+* and *+>kir2.1*) larvae (**Figure 5B, C**), whereas the timing of larva-pupa transition (pupariation) was hardly affected (**Figure 5D**). Similar results were obtained in larvae following *Crz* RNAi-mediated knockdown in Crz neurons and *Crz* loss-of-function genetic mutants (**Figure 5C**). Furthermore, larvae with inhibited Crz neuronal activity grew faster than control larvae during the L3 stage as indicated by growth-rate measurements (**Figure 5E**). These data suggested that Crz neurons negatively control systemic body growth by affecting the growth rate during the L3 stage.

The basal ecdysteroid level increases during the mid-L3 stage, modulating the body growth rate prior to pupariation [38]. To examine whether Crz neurons affect basal ecdysteroid biosynthesis, I measured ecdysteroid levels by liquid chromatography/mass spectrometry (LC-MS/MS) in collaboration with Dr. Takashi Nishimura (RIKEN Center for Biosystems Dynamics Research) [39–42]. I collected larvae at L3 ecdysis to synchronize developmental timing. This approach allowed us to accurately quantify a relatively low titer of 20-hydroxyecdysone (20E), the active form of ecdysteroid.

At 22, 26, and 30 h after L3 ecdysis, I detected a small increase in the levels of 20E in control larvae (**Figure 6A**), which corresponds to the increase in 20E prior to the peak level

characteristic for pupariation [38]. Interestingly, the timing of the small 20E increase was delayed in *Crz>kir2.1* larvae (**Figure 6B**). In contrast, the peak level of 20E was not significantly different between *Crz>kir 2.1* and control larvae in the late-L3 stage (56 h after L3 ecdysis, **Figure 6A, B**). Taken together, these data strongly indicated that Crz neurons regulate systemic body growth by controlling the timing of basal ecdysteroid biosynthesis during the mid-L3 stage.

Regulation of systemic body growth requires *Wts/Yki/ban* signaling in the PG (**Figure 1B**) [11,12]. Overexpression of the microRNA *ban* induces body overgrowth, reminiscent of the *Crz* loss-of-function phenotype. Therefore, I next asked whether Crz neurons affect *ban* activity during the mid-L3 stage. When *ban* expression was analyzed in the PG using a *ban-lacZ* reporter, *Crz>Crz-RNAi* larvae exhibited a dramatic increase in *ban-lacZ* signal at 72 h after hatching (hAH) (**Figure 7**). These data strongly suggested that the regulation of basal ecdysteroid biosynthesis by Crz neurons is related to *ban* activity in the PG.

Crz neurons have neuronal connections with PTTH neurons as well as PG cells

To examine whether Crz peptides are received by the PG, I obtained a GAL4 knock-in fly strain, *CrzR::2A::GAL4* from Dr. Shu Kondo (National Institute of Genetics) and Dr. Hiromu Tanimoto (Graduate School of Life Sciences) on a collaboration basis. In *CrzR::2A::GAL4*, a transgene containing the 2A peptide sequence and GAL4 was inserted immediately upstream of the stop codon of *CrzR* (**Figure 8A**) [43]. GFP signals driven by *CrzR::2A::GAL4* were detected in a large area of the brain, including neurons that project to the PG (**Figure 8B**). Unexpectedly, *CrzR* was not expressed in the PG cells, while being expressed in neurons projecting to the PG (**Figure 8C**). From their characteristic anatomical structure, these neurons are predicted to be PTTH neurons. Based on this hypothesis, I performed immunostaining with anti-PTTH antibodies. Anti-PTTH signal was observed in the axon termination of PG-innervating neurons labeled by *CrzR::2A::GAL4* (**Figure 8C**). This suggests that *CrzR* was expressed in PTTH neurons instead of PG cells.

To explore the spatial relationship between PTTH and Crz neurons, I visualized both these cell types simultaneously (**Figure 9A, B**). PTTH and Crz neurons appear to share the same tract and are closely located in the PG (**Figure 9C**). In addition, I performed GRASP analysis, in which two complementary fragments of GFP were expressed in PTTH and Crz neurons, respectively. GFP reconstruct signals appeared both in the brain and PG (**Figure 10A**). Consistent with the GRASP analysis results, CATMAID analysis revealed the presence of presynaptic sites and DCVs at the contact sites between PTTH and Crz neurons (**Figure 10B, C**). Notably, these DCV fusion sites were localized to the axons of PTTH and Crz neurons in the PG. The connectivity between PTTH and Crz neurons was bidirectional

(Figure 10D). Taken together, these data strongly supported that Crz neurons are connected with PTTH neurons at their axons.

Crz receptor functions in PTTH neurons

I hypothesized that Crz neurons regulate systemic growth through CrzR and its downstream signaling in PTTH neurons. To test this hypothesis, I silenced *CrzR* in PTTH neurons by RNAi. Knockdown of *CrzR* in PTTH neurons resulted in an increase in pupal size, whereas it had little effect on the timing of pupariation. Similar results were obtained in *CrzR* loss-of-function genetic mutants **(Figure 11A)**, indicating that inhibition of Crz neuronal activity and inhibition of CrzR in PTTH neurons induce the same phenotype **(Figure 11B)**. Taken together, these results strongly supported the hypothesis that Crz neurons transmit Crz to PTTH neurons via CrzR and negatively regulate systemic growth via PTTH signals.

PTTH neurons are highly sensitive to Crz peptides during the middle L3 stage

PTTH neurons innervate the PG and stimulate ecdysteroid production [16]. The dendrites of PTTH neurons contact the axons of pigment-dispersing factor (PDF)-producing neurons, and PDF influences the transcriptional periodicity of *ptth*, suggesting that PTTH neurons are affected by the circadian rhythm [16]. In addition, *Lgr3* neurons and allatostatin A (*AstA*)-producing neurons contact PTTH neurons, controlling the timing of the peak in ecdysteroid biosynthesis during pupariation. Alteration of the activity of PTTH, *Lgr3*, and *AstA* neurons changes pupariation timing; thus, these neurons regulate the timing of maturation by regulating peak ecdysteroid biosynthesis [44–49]. In contrast, recent studies have suggested a role of PTTH signaling in basal ecdysteroid production, in which *Wts/Yki/ban* signaling is essential in the PG [7–9,11,12]. This implies that PTTH neurons have dual roles in generating both basal and peak levels of ecdysteroid. However, contrary to the neuronal regulation of peak ecdysteroid biosynthesis, it remains unclear whether there are neuronal mechanisms that modulate the activity of PTTH neurons for basal ecdysteroid biosynthesis **(Figure 12A)**.

Under such circumstances, this study suggests that Crz neurons affect PTTH neurons to promote basal ecdysteroid biosynthesis but not peak levels. It remained unclear how Crz neurons regulate PTTH neurons to adjust basal ecdysteroid biosynthesis. As inhibition of Crz neuronal activity or CrzR in PTTH neurons affected systemic growth, but not the pupariation timing, I next sought to elucidate whether the sensitivity of PTTH neurons to Crz changes in a stage-specific manner. To this end, I observed *CrzR* expression in PTTH neurons by measuring the fluorescence intensity of GFP driven by *CrzR::2A::GAL4*. Strong GFP signals were observed during the mid-L3 stage, whereas GFP signals were significantly reduced during the late-L3 stage **(Figure 12B, C)**. These results suggested that *CrzR* is

highly expressed in PTTH neurons, so that Crz peptide affects PTTH neurons more effectively during the mid-L3 stage.

To directly monitor the sensitivity of PTTH neurons to Crz, I utilized the genetically encoded calcium indicator, GCaMP6s (**Figure 13A**) [50]. Because CrzR is a member of the gonadotropin-releasing hormone (GnRH) receptor superfamily, its signaling pathway generally involves calcium ions as second messengers (**Figure 13A**) [51,52]. I dissected the brains of *PTTH>GCaMP6* larvae and cultured them in Schneider's *Drosophila* Medium (SDM). Then, synthetic Crz peptides were administered to cultured brains and GCaMP6s activity was monitored in the cell body of PTTH neurons by laser-scanning confocal microscopy (**Figure 13B**). A strong calcium response was observed in PTTH neurons of larvae during the mid-L3 stage. Interestingly, the calcium response was significantly reduced during the late-L3 stage (**Figure 13C, D**). Furthermore, I monitored GCaMP6s activity in PTTH neurons after activation of Crz neurons by the red-light-gated cation channel CsChrimson [53]. CsChrimson was activated in the cell body of Crz neurons by red light irradiation, then GCaMP6s activity was monitored in the cell body of PTTH neurons (**Figure 13E**). A strong calcium response was observed during the mid-L3, but not the late-L3 stage (**Figure 13F**). Taken together, these results strongly suggested that Crz neurons affect PTTH neurons only during the mid-L3 stage. These results are consistent with the expression pattern of *CrzR* in PTTH neurons.

Crz neuronal activity is regulated by octopamine neurons in the sub-esophageal zone

To understand the type of signals received by Crz neurons for regulating systemic growth, I aimed to analyze signals upstream of Crz neurons. While screening GAL4 strains with labeled PG-innervating neurons in the Janelia GAL4 collection [22–24], I found that *R50A06-GAL4* is expressed in Crz neurons. Because *R50A06-GAL4* carries the *GAL4* cassette fused with an upstream fragment of *Oamb* (encoding Octopamine receptor in mushroom bodies) as a promoter [54] (**Figure 14A**), I assumed that *Oamb* is expressed in Crz neurons. Octopamine is the invertebrate analog of adrenergic ligands [55–57].

To test this hypothesis, I obtained *Oamb::2A::GAL4* flies and conducted immunohistochemical analysis with anti-Crz antibodies. GFP signals driven by *Oamb::2A::GAL4* were observed in the cell body of Crz neurons (**Figure 14B**). To explore whether *Oamb* is involved in the regulation of systemic growth by Crz neurons, I silenced *Oamb* in Crz neurons through RNAi. Knockdown of *Oamb* in Crz neurons resulted in an increase in pupal size, whereas it had little effect on pupariation timing, phenocopying the inhibition of Crz neuronal activity (**Figure 14C, D**). These data suggested that octopamine signaling regulates Crz neuronal activity on systemic growth.

To elucidate which octopamine-producing neurons (octopamine neurons) innervate Crz neurons, I visualized octopamine neurons in the *Tdc2-GAL4* strain as tyrosine decarboxylase 2 (*Tdc2*) is a key enzyme in octopamine biosynthesis [58]. A number of octopamine neurons appeared to extend their axons to the dendrites of Crz neurons in the subesophageal zone (SEZ) (**Figure 15A**). The SEZ of the *Drosophila* brain processes mechanosensory and gustatory sensory input from sensilla located on the head, mouth cavity, and trunk [59]. When I subjected the *Tdc2-GAL4* and *Crz-LexA* strains to GRASP analysis, reconstituted GFP signals were detected in the dendritic zone of Crz neurons in the SEZ (**Figure 15B**). Inhibition of octopamine neuronal activity through tetanus toxin light chain (*TeTxLC*) expressing as well as *Tdc2* knockdown resulted in an increase in pupal size, whereas their effect on pupariation timing was very limited (**Figure 15C**). Knockdown of *TbH* encoding Tyramine β hydroxylase, which catalyzes the conversion Altogether, these results suggested that octopamine-mediated signaling regulates the activity of Crz neurons on systemic growth.

Involvement of Crz neurons in the crosstalk between basal ecdysteroid levels and Dilp in growth regulation

In animals, the conserved insulin/insulin-like growth factor signaling pathways play central roles in regulating metabolism and systemic growth [61]. *Drosophila* produces several insulin-like peptides (Dilps) in specialized insulin-producing cells (IPCs) in the brain, which is the main source of circulating insulin. Release of insulin from IPCs is regulated in response to nutritional information relayed through the fat body, a functional equivalent of the mammalian liver and adipose tissue [62–67]. Circulating insulin promotes larval body growth as well as ecdysteroid. Therefore, I tested the possibility that Crz neurons regulate Dilp secretion from IPCs to explore the crosstalk between basal ecdysteroid levels and Dilp in growth regulation. Simultaneous visualization of Crz neurons and IPCs pointed that they share the same tract in the brain (**Figure 16A**). Furthermore, knockdown of *CrzR* in IPCs increased pupal size (**Figure 16B**). Consequently, I measured anti-Dilp2 intensity in IPCs of larvae following inhibition of Crz neurons. Crz neurons were inhibited by expressing *kir2.1* or knockdown of *Crz* in Crz neurons, which led to a significant decrease in anti-Dilp2 signals in IPCs during the mid-L3 stage (**Figure 16C, D**). These results suggested that Crz neurons negatively control growth by regulating Dilp2 secretion from IPCs in addition to regulating basal ecdysteroid level.

Discussion

Coordination of systemic body growth and maturation by Crz signaling

This study elucidated that Crz neurons negatively control systemic growth by regulating basal ecdysteroid biosynthesis via PTTH neurons. Crz neurons affect PTTH neurons only during the mid-L3 stage, as *CrzR* expression level in PTTH neurons varies depending on the stage (**Figure 17**).

Previous studies showed that silencing Wts signaling in the PG reduced the basal level of ecdysteroids [8,12]. In contrast, inhibiting Crz neurons just delayed basal ecdysteroid slight elevation. While previous reports used ELISA and phased larvae at egg laying, I used LC-MS/MS and phased larvae at L3 ecdysis, which allowed me to detect a relatively low titer of 20E. As the reduction of 20E titer is also observed in my data, there is a possibility that the decrease in 20E titer previously observed reflected a delay of slight elevation of basal ecdysteroids. When I measured pupariation timing or pupal size, I phased larvae at egg laying. Phasing larvae at L3 ecdysis for all of the experiments as well may show the strict relationship between ecdysteroid titer and growth/maturation.

It was also suggested that Crz neurons control growth by regulating Dilp2 secretion from IPC during the middle L3 stage (**Figure 18**). Insulin signals promote systemic growth and ecdysteroid production in the PG. Wts signal in the PG couples insulin signaling with ecdysteroid biosynthesis to adjust systemic growth and coordinate growth between tissues in response to nutrient availability during development [12]. It is possible that Crz neurons coordinate growth between tissues, and consequently prevent overgrowth under conditions associated with high insulin signaling.

Environmental nutritional/taste cues input the Crz signaling pathway

This study suggested that octopamine-mediated signaling regulates the activity of Crz neurons in systemic growth (**Figure 18**). Although I was unable to locate the cell body of octopamine neurons, the contact sites were close to the SEZ, which has been suggested to act as a feeding control center [17,68]. Considering that basal ecdysteroid biosynthesis increases after larvae gain the critical weight [38], Crz neurons may receive nutritional or taste cues via octopamine neurons. This corresponds to larvae that feed during the mid-L3 stage in which Crz neurons affect PTTH neurons, while larvae wander to seek pupariation place during the late-L3 stage. Accordingly, silencing of *Crz* in Crz neurons reportedly reduced the pupariation ratio under nutrient restriction [69]. Such a neuronal network relay underlies the pulses of ecdysteroid synthesis, which is tightly coupled to environmental nutritional information. However, it remains largely unclear how such cumulative nutritional

information converges into the growth rate prior to maturation. It would be crucial to address whether octopamine neurons are activated in response to environmental cues.

Direct function of Crz neurons in the PG on ecdysteroid biosynthesis

So far it remains unclear how Crz neurons affect the PG directly and what function Crz neurons play in this pathway (**Figure 18**). While CrzR::2A>GFP signal was not detected in PG cells, connectome analysis clearly indicated that presynaptic density and DCVs of Crz neurons were in contact with PG cells (**Figure 4C, 8C**). To explain the discordant findings on CrzR-mediated signaling, I reasoned that Crz neurons may transmit other neuropeptides to the PG or PG cells may express other receptors that receive Crz peptides. Short neuropeptide F (sNPF) is produced and functions as a neuropeptide in a group of Crz neurons [70]. However, immunohistochemical analysis revealed that sNPF was not localized in PG-projecting Crz neurons (**Figure 19A, B**). Therefore, I concluded that Crz neurons do not secrete sNPF to the PG. It would be intriguing to assess whether Crz neurons secrete several types of neuropeptides to transmit signals to distinct targets, including PG cells and PTTH neurons, to modulate ecdysteroid biosynthesis.

Evolutionarily conserved neuronal circuitry controls developmental transition

In vertebrates, the onset of puberty follows steroid hormone biosynthesis under the control of the hypothalamic-pituitary-gonadal (HPG) axis [71,72]. In the hypothalamus, kisspeptin (KISS) acts on GnRH neurons [73–77]. GnRH secretion induces the secretion of luteinizing hormone (LH) and follicle-stimulating hormone (FSH) from the pituitary gland, leading to reproductive maturation in the gonads [78]. Therefore, the regulation of KISS and GnRH secretion is crucial for steroid hormone biosynthesis and puberty initiation (**Figure 20**).

This study provides evidence showing that Crz neurons directly affect PTTH neurons via CrzR signaling. Crz and CrzR are homologous to GnRH and GnRH receptor, respectively [79]. Moreover, a recent study reported that AstA and AstA receptor 1, which are homologous to KISS and KISS receptor, control the onset of maturation by promoting PTTH secretion and promote growth by controlling Dilp secretion from IPCs [45]. Based on my results and previous studies, I suggest that the two phases of ecdysteroid biosynthesis are differentially regulated by two neuronal pathways: Crz/GnRH neurons control initial, basal ecdysteroid biosynthesis, whereas AstA/KISS neurons control peak ecdysteroid biosynthesis. These neuronal systems would increase the temporal resolution of activity of PTTH neurons, reflecting to the timing of basal and peak ecdysteroid biosynthesis. Fine tuning of the neuronal network of PTTH and Crz neurons, as well as PDF neurons, IPCs, Lgr3 neurons,

and AstA neurons contribute to pulsatile two-step ecdysteroid synthesis in a stage-specific manner (**Figure 20**).

These findings suggest an evolutionarily conserved neuronal circuitry for controlling the developmental transition from the juvenile to adult stage [79]. Given the HPG axis in vertebrates and the relationship between GnRH and KISS, investigating the potential crosstalk between Crz neurons and AstA neurons in controlling PTTH neurons will be important to understand how an evolutionarily conserved neuronal circuitry is customized to insect development in response to environmental cues.

Conclusions

I believe that Crz signaling, as well as GnRH signaling, has a role in initiating maturation, as sexual maturation and appropriate body size impact the survival fitness and reproductive success during the adult stage. Based on complementary findings, I propose that the Crz-PTTH neuronal axis regulates basal ecdysteroid biosynthesis. Furthermore, this study suggested that Crz neuronal activity is regulated by octopamine neurons in the SEZ in response to environmental nutritional or taste cues. However, further research will be needed to better understand the function of Crz neurons in response to environmental cues. Contrasting to other neurons that have been reported to regulate ecdysteroid biosynthesis (PTTH, AstA, Lgr3, and SE0_{PG} neurons), Crz neurons are the only neurons that do not affect pupariation timing, but affect systemic growth. In addition, Crz neurons are essential for the regulation of basal ecdysteroid biosynthesis, which is clearly delimited from peak ecdysteroid biosynthesis. Most significantly, this study uncovered a neuronal regulatory system affecting ecdysteroid biosynthesis, thus coordinating growth and maturation in a developmental stage-specific manner.

Methods

***Drosophila* strains and maintenance**

The following strains were provided by the Bloomington *Drosophila* Stock Center (BDSC): *hs-FLP* (#1929), *UAS-{FRT stop} mCD8::GFP* (#30125), *LexAop-CD4::spGFP₁₁*, *UAS-CD4::spGFP₁₋₁₀* (#58755), *Crz-GAL4* (#51977), *UAS-Kir2.1* (#6596), *Df(3L)BSC730* (#26828), *UAS-GCaMP6s* (#42746), *LexAop-mCherry* (#52272), *GMR50A06-GAL4* (#38722), *UAS-Oamb-IR* (#31233), *Tdc2-GAL4* (#9313), *UAS-TeTxLC* (#28838), *UAS-Tdc2-IR* (#25871), *UAS-TbH-IR* (#27677). The following strains were provided by the *Drosophila* Genetics Resource Center (DGRC): *Df(3R)ED5644* (#150163), *NP0394-GAL4* (#103604). The following strains were provided by the Vienna *Drosophila* RNAi Center (VDRC): *UAS-Crz-IR* (#30670), *UAS-CrzR-IR* (#44310). *LexAop-CsChrimson::mVenus*; *UAS-GCaMP6s* (#3020396) was provided by the Janelia Research Campus. *phm-GAL4*, *PTTH-GAL4*, and *PTTH-HA* (gifts from M.B. O'Connor, University of Minnesota) [16], *Crz-LexA* (gift from Y. Ohhara as collaboration, University of Shizuoka) *bantam-lacZ* (a gift from K. F. Rewitz, University of Copenhagen) [12], *Crz^{SK2-5}* (gift from S. Kondo as collaboration, National Institute of Genetics), *CrzR::2A::GAL4* and *Oamb::2A::GAL4* (gifts from S. Kondo, National Institute of Genetics and H. Tanimoto, Tohoku University, as collaboration), *Dilp2-GAL4* (gift from T. Nishimura, RIKEN Center for Biosystems Dynamics Research) [80], *UAS-GFP*; *UAS-mCD8::GFP* (a gift from K. Ito, The University of Cologne) [81], *Crz-GAL4(JHP)* and *CrzR⁰¹* (gifts from J. H. Park, University of Tennessee) [82] were as described.

Flies were reared on 0.275 g agar, 5.0 g glucose, 4.5 g of cornmeal, 2.0 g yeast extract, 150 μ L propionic acid, and 175 μ L butylparaben in 50 mL water. Experiments were conducted at 25°C under a 12:12-h light/dark cycle. *w¹¹¹⁸* was used as the wild type. Heterozygous controls were obtained by crossing *w¹¹¹⁸* to strains of GAL4 driver or UAS effector. For all experiments, both males and females were used.

Immunohistochemistry and imaging

Larvae were dissected at the appropriate developmental stage and fixed with 3.7% formaldehyde with 0.05% Triton X-100 at room temperature for 30 min [83]. The following primary antibodies were used: anti-Crz (rabbit, 1:200, a gift from Jan A. Veenstra, University of Bordeaux) [84], anti-Sro (guinea pig, 1:1,000) [17], and anti-GFP (rabbit, 1:1000, Thermo Fisher Scientific; mouse, 1:300, Sigma), anti-LacZ (mouse, 1:300, Promega), anti-HA (mouse, 1:1000, Abcam). Anti-PTTH antibody (rabbit, 1:1000) was a gift from Nuria Romero and Pierre Leopold (unpublished, [85]), anti-Dilp2 (guinea pig, 1:1000) was a gift from Takashi Nishimura [80]. Alexa Fluor 488/555-conjugated secondary antibodies were

purchased from Thermo Fisher Scientific (1:200). Samples were visualized under an LSM 700 confocal microscope (Carl Zeiss).

Neuronal reconstruction and output compartments of Crz neurons

Reconstructions were based on a serial section transmission electron microscope data set comprising the entire central nervous system and the RG of an L1 larva ($n=1$) [34]. This data set has been generated as described previously [86]. Neuronal skeletons were manually reconstructed using a modified version of CATMAID [31,87] and underwent two rounds of reviews. Crz neurons and PTTH neurons were identified by reconstructing all neurosecretory cells that target to the PG and were compared with the known locations of these cells [15] and staining data. DCVs containing peptides were marked in the PG, PTTH neurons, and Crz neurons, when being fused to the cell membrane (DCV fusion sites). These sites had in many cases no corresponding postsynaptic sites in adjacent neurons or endocrine cells. Fusion of DCVs indicates neuroendocrine release of peptides (Hückesfeld et al., unpublished results).

FLP-out analysis

To generate mitotic clones in PG-innervating Crz neurons, larvae were collected at different times (hAH) and heat-shocked at 37 °C for 90 min. I found that heat-shocking larvae at 48 hAH generates a single-cell clone expressing GFP.

Pupal length and growth rate measurements

For growth-rate experiments, synchronized larvae were collected at different time points during the L3 stage. The larvae were transferred into a 1.5-mL tube containing PBS and exposed to 60°C for 1 min to stretch them out for precise length measurements. Larval and pupal sizes were determined from images captured with a camera attached to a dissection microscope (S8AP0, Leica). Images were processed using ImageJ v. 1.47 [88].

Developmental timing experiments

Egg laying was induced on 3% agar plates containing 30% grape-juice (Welch) at 25°C. Newly hatched larvae were collected into small vials (20 larvae each) and raised on ground fly food. Pupae were counted at the indicated time points after hatching. Per genotype, four tubes were scored two times a day. Pupariation timing was calculated in Microsoft Excel using non-linear regression curve fitting.

Quantification of ecdysteroids by LC-MS/MS

Approximately 22 h after egg laying, newly hatched L1 larvae were collected. To minimize differences in developmental progression during the L3 stage, I collected L2 larvae at 48 hAH and allowed them to molt in 2 h intervals. Synchronized L3 larvae were collected within 2 h after L3 ecdysis. Ecdysteroids were quantified as described previously, with some modifications [38]. Samples were collected in 1.5-mL tubes and weighed using a microbalance (Sartorius). Then, the samples were homogenized in 200 μ L of cold methanol with a pestle and centrifuged at $20,000 \times g$ at 4°C for 5 min. This procedure was repeated. The supernatant was mixed with 300 μ L of methanol, 500 μ L of H_2O , and 200 μ L of CHCl_3 , and vortexed at room temperature for 20 min. The samples were centrifuged at $20,000 \times g$ at 4°C for 15 min, and the aqueous phase was collected and dried in a vacuum concentrator. The dried material was re-dissolved in 400 μ L of 10% methanol containing 100 pg muristerone A (MuA, internal standard). The samples were loaded on MonoSpin C18 columns (GL Sciences Inc.). The columns were pre-washed with 200 μ L of methanol and water. After sample loading and centrifugation at $3,000 \times g$ for 1 min, the columns were washed with 400 μ L of 10% methanol. The samples were eluted with 400 μ L of 60% methanol. The eluates were dried, re-dissolved in 10 % methanol, and analyzed by LC-MS/MS.

Chromatographic separation was carried out on an ACQUITY BEH C18 column (50 mm \times 2.1 mm, 1.7- μ m particles, Waters) in combination with a VanGuard precolumn (5 mm \times 2.1 mm, 1.7- μ m particles) using an Acquity UPLC H-Class System (Waters). The mobile phase consisted of solvent A, 0.1 % formic acid in acetonitrile, and solvent B, 0.1% formic acid in H_2O , and was delivered at a flow rate of 0.25 ml/min at 40°C . Linear gradients were as follows: 15% A at 0–0.5 min, 15–40% A at 0.5–2 min, 40% A at 2–2.5 min, and 15% A at 2.5–5 min. Mass spectrometry analysis was conducted using a Xevo TQD triple quadrupole mass spectrometer (Waters) coupled with an electrospray ionization source in the positive ion mode. The MRM transitions were as follows: 20E, m/z 481.2 \rightarrow 165.2 and 371.3; MuA, m/z 497.3 \rightarrow 297.2 and 425.3. Analytical conditions were optimized using standard solutions of 20E (Sigma) and MuA (AG Scientific). Sample concentrations were calculated from a standard curve obtained from serial dilutions of each standard and then normalized to an internal standard. The values were also normalized to larval wet weight.

Quantification of GFP signals in the axons of PTTH neurons

The brain-RG complexes were dissected from *CrzR::2A::GAL4>GFP* larvae during the mid- (72 hAH) or late- (96 hAH) L3 stage. Confocal Z-stack images of the RG were acquired with identical laser power and scanning settings. The mean fluorescence intensity of GFP signals in the PG area was quantified. In each experiment, the values were normalized to the average of the control.

Calcium imaging of PTTH neurons administered Crz peptide

Calcium transients in PTTH neurons were imaged in flies expressing two copies of *UAS-GCaMP6s* driven by *NP0394-GAL4*. The brain-RG complexes were dissected in PBS at the appropriate time point (mid- or late-L3 stage). Imaginal discs were removed from the brain. Dissected brains were immersed in 50 μ L of Schneider's *Drosophila* Medium (SDM, GIBCO) and fixed on the bottom of a glass-bottom dish (35 \times 10 mm, IWAKI) with insect pins (0.18-mm diameter, Shiga) and silicone grease (BECKMAN). Custom-synthesized Crz peptide amidated at its C-terminus and pyrrolidinated at its N-terminus (pyr-TFQYSRGWTN-CONH₂) was synthesized by Eurofins Genomics. The synthesized Crz peptide was diluted in SDM to 2 nM. 50 μ l of SDM with or without 2 nM of Crz peptide was added directly into the dish containing 50 μ l of SDM, yielding a final concentration of 1 nM Crz peptide. Live imaging was performed with a laser-scanning confocal microscope (LSM700, Carl Zeiss) with a 40 \times water-immersion objective lens. GCaMP6s was excited with the 488-nm laser. Time-lapse images were acquired every 2 seconds for 10 min. For image processing, a single-cell body of a PTTH neuron was selected in a region of interest (ROI) over multiple time frames. Mean fluorescence intensities were measured along the time axis using ImageJ. Data were analyzed in Microsoft Excel.

Calcium imaging of PTTH neurons with CsChrimson activation

Calcium transients in PTTH neurons were imaged in flies expressing *UAS-GCaMP6s* driven by *NP0394-GAL4* and *LexAop-CsChrimson* driven by *Crz-LexA*. Newly hatched larvae were raised on food containing 0.1 mM all-trans retinal (Sigma) in the dark. Flies were prepared for calcium imaging as described above, and were irradiated with 7 pulses of red laser (633 nm) every 4 s in each experiment.

Quantification of anti-Dilp2 signals in the cell body of IPCs

The brain-RG complexes were dissected from *Crz>kir2.1* or *Crz>Crz-IR* larvae during the mid- L3 stage (72 hAH). Confocal Z-stack images of the brain were acquired with identical laser power and scanning settings. The mean fluorescence intensity of Dilp2 signals in the IPCs was quantified. In each experiment, the values were normalized to the average of the control.

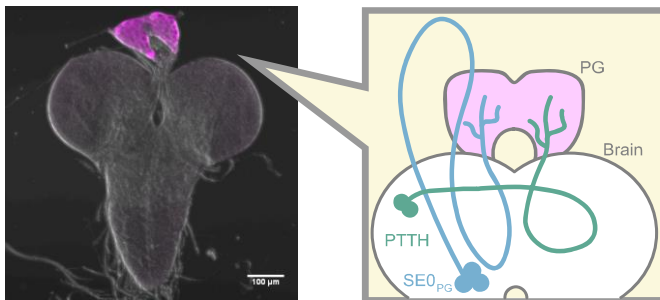
Quantitative statistical analysis

All experiments were performed at least 3 times independently. Data on larval/pupal size, ecdysteroid levels, and Dilp2 intensity values were analyzed by the Tukey–Kramer test. GFP

intensity values were compared by Mann–Whitney U test. Calcium responses in PTTH neurons were analyzed by Kolmogorov–Smirnov test. Sample sizes were chosen based on the number of independent experiments required for statistical significance and technical feasibility. The experiments were not randomized, and the investigators were not blinded. All statistical analyses were carried out using the “R” software (R Foundation for Statistical Computing, Vienna, Austria). $P \leq 0.05$ was considered significant. P -values are provided in comparison with control as $*P \leq 0.05$, $**P \leq 0.01$, $***P \leq 0.001$, and “n.s.” for non-significant ($P > 0.05$).

Figures

A



B

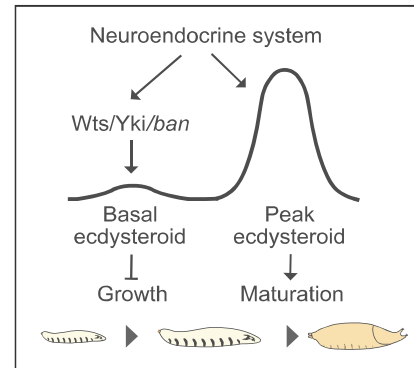
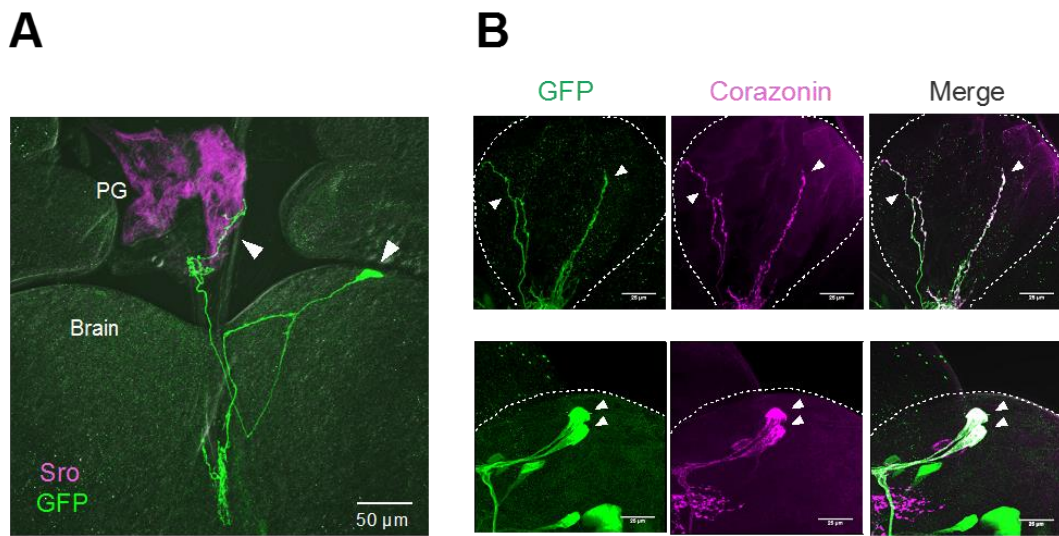


Figure 1

Ecdysteroid is biosynthesized in the prothoracic gland (PG) and regulated by the neuronal regulatory mechanism.

(A) Anatomical position of the PG (magenta) and projections of PTTH (green) and SE0_{PG} neurons (blue) to the PG. Left: the ring glands-brain complex from *w¹¹¹⁸* larva with Shroud (Sro) antibody staining (magenta) of PG cells. Right: Schematic diagram showing only one side of PTTH and SE0_{PG} neurons for simplicity. Scale bar: 100 μm. (B) Schematic diagram depicting the roles of the neuroendocrine system in ecdysteroid biosynthesis. While the endocrine system affects *Wts/Yki/ban* signaling to promote basal ecdysteroid biosynthesis that inhibits growth, it also regulates peak ecdysteroid biosynthesis, which triggers maturation.



GMR41A04>hsFLP, (FRT stop)mCD8::GFP

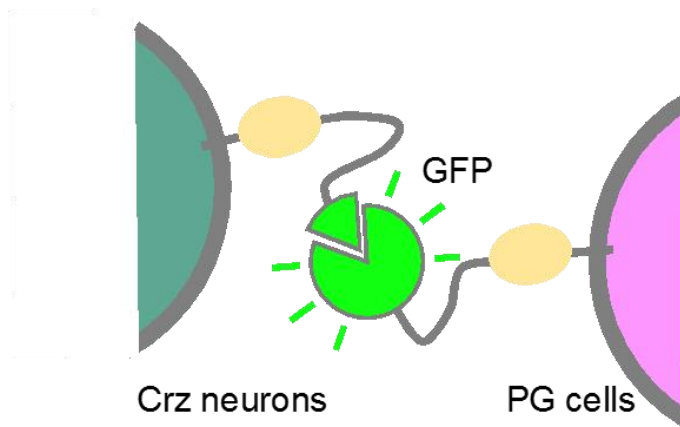
GMR41A04>GFP, mCD8::GFP

Figure 2

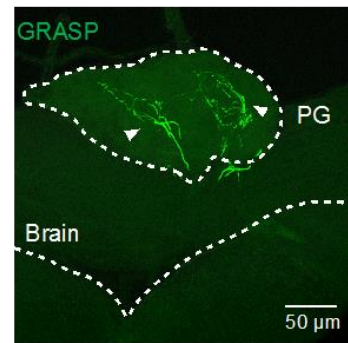
Identification of PG-innervating Corazonin producing neurons

(A) FLP-out GAL4 clone using *R41A04-GAL4* driver labeled single neurons in one side of brain hemisphere (arrowheads). The clone expressed mCD8::GFP (green) and sent projections toward the PG (anti-Sro, magenta). Scale bar: 50 μ m.

(B) mCD8::GFP signals (green) driven by *R4104-GAL4* and anti-Corazonin signals (magenta) were merged both in the axon termination projecting to the PG and in the cell body. Scale bar: 25 μ m.

A**B**

GRASP (Crz-PG)



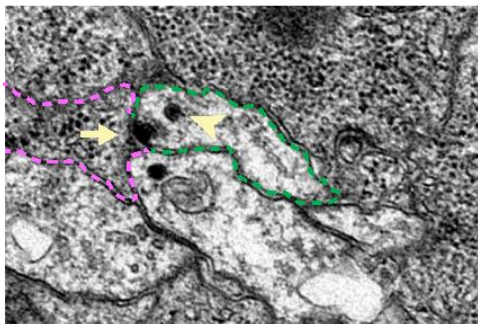
Crz>CD4::spGFP₁₁
phm>CD4::spGFP₁₋₁₀

Figure 3**GRASP analyses revealed synaptic connections between Crz neurons and PG cells**

(A) Schematic diagram depicting the GFP Reconstitution Across Synaptic Partners (GRASP) analysis in which two complementary fragments of GFP were expressed in Crz neurons and PG cells, respectively.

(B) *CD4::spGFP₁₁* was expressed by *Crz-LexA*, whereas *CD4::spGFP₁₋₁₀* was expressed by *phm-GAL4*. Scale bar: 50 μm.

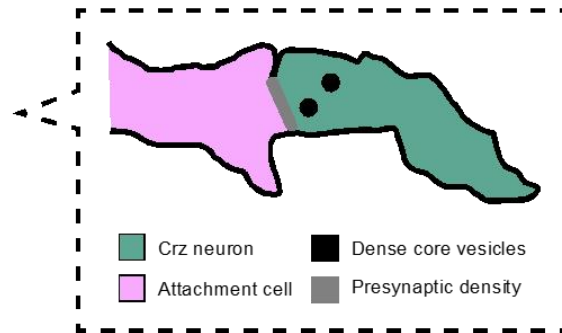
A Typical synapses with DCV



500 nm

Crz neuron onto PG cell

B Schematic drawing of DCV fusion site



C Connectivity diagram

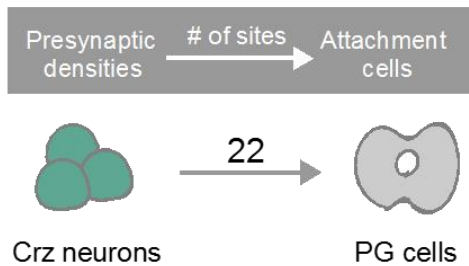


Figure 4

Investigating the connections of Crz neurons with PG cells at the ultrastructural level

(A) Representative electron-microscopy micrographs of DCV fusion sites, in which Crz neurons connect to PG cells. Presynaptic densities and DCVs are indicated by arrows and arrowheads, respectively. Scale bar: 500 nm.

(B) Schematic illustration of a DCV fusion site with presynaptic density (grey bar) and DCVs (black circles). Crz neurons (green) contact PG cells (pink).

(C) Connectivity diagram between Crz neurons and PG cells. Numbers describe the contact site count marked by presynaptic densities.

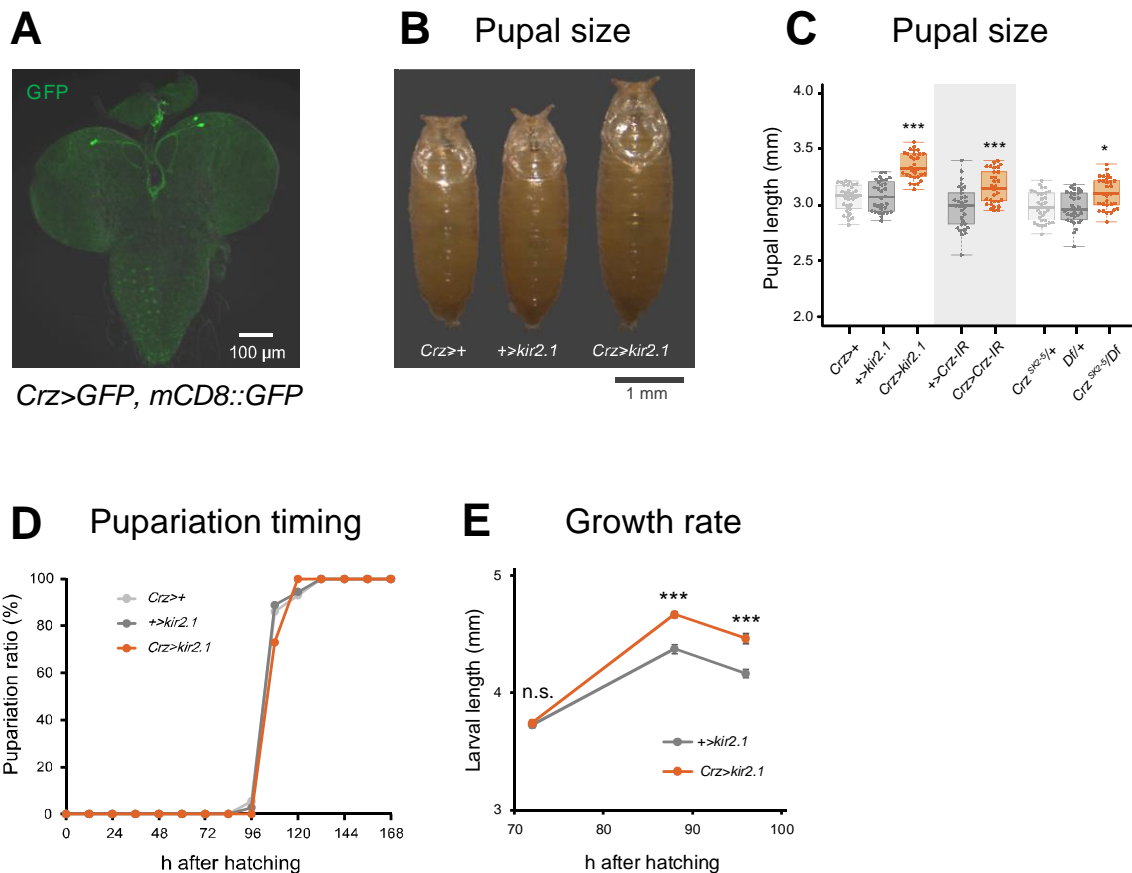


Figure 5

Function of Crz neurons on pupal size and pupariation timing

(A) GFP and mCD8::GFP signals (green) driven by *Crz-GAL4* from Bloomington Drosophila stock center (#51977). Scale bar: 100 μ m.

(B) Representative images of control (*Crz>+* and *+>kir2.1*) and *Crz>kir2.1* pupae. Inhibition of Crz neuronal activity increased pupal size. Scale bar: 1 mm.

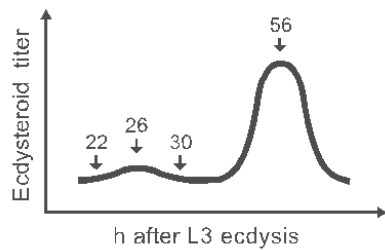
(C) Quantitative analysis of pupal length in control (*Crz>+*, *+>kir2.1*, *+>Crz-IR* and *Crz^{SK2-5/+}*, *Df/+*) and Crz-deficient (*Crz>kir2.1*, *Crz>Crz-IR* and *Crz^{SK2-5/Df}*) larvae.

(D) Pupariation timing of control (*Crz>+* and *+>kir2.1*) and *Crz>kir2.1* larvae.

(E) Growth rate during the L3 stage of control (*+>kir2.1*) and *Crz>kir2.1* larvae.

Tukey–Kramer test was used for data in panels C, E, and F. *** $P \leq 0.001$, ** $P \leq 0.01$, and * $P \leq 0.05$; n.s., non-significant ($P > 0.05$).

A Ecdysteroid fluctuations



B Ecdysteroid titer

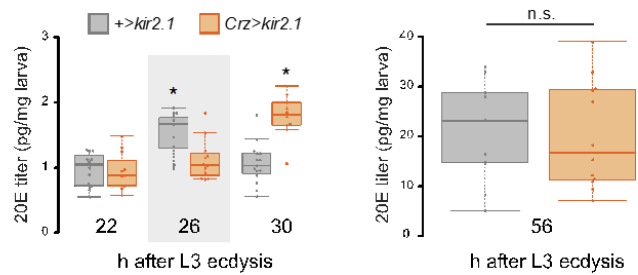


Figure 6

Measurement of ecdysteroid titer in larvae following inhibition of Crz neurons

(A) Schematic drawing of fluctuations in hemolymph ecdysteroid levels during the L3 stage. Ecdysteroid levels are basal during the mid-L3 stage (22, 26, and 30 h after L3 ecdysis), and peak during the late-L3 stage (56 h after L3 ecdysis). A small increase in ecdysteroid was observed during the mid-L3 stage.

(B) 20E titer in control (+>kir2.1) and Crz>kir2.1 larvae during the mid-L3 stage (22, 26, and 30 h after L3 ecdysis) and the late-L3 stage (56 h after L3 ecdysis). Tukey–Kramer test was used for data in panels B. *** $P \leq 0.001$, ** $P \leq 0.01$, and * $P \leq 0.05$; n.s., non-significant ($P > 0.05$).

bantam-lacZ signal

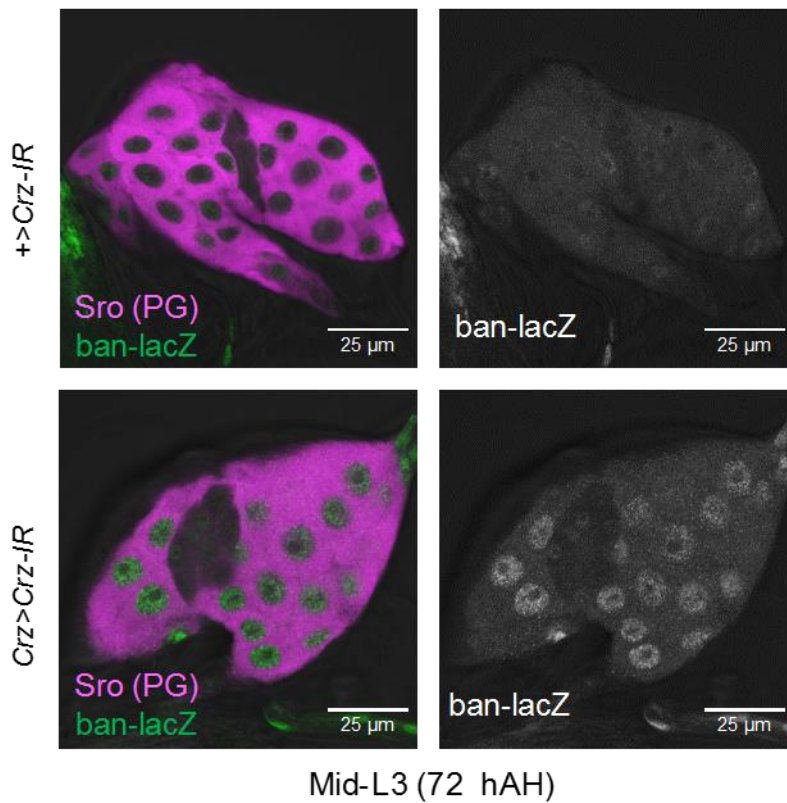


Figure 7

Observation of bantam signals in *Crz* neurons of *Crz* knockdown larvae

PGs from control (+>*Crz-IR*) and *Crz*>*Crz-IR* larvae expressing a *ban-lacZ* reporter (green) during the mid-L3 (72 hAH) stage. PG cells were labelled with anti-Shroud (Sro) antibody (magenta). hAH; hours after hatching. Scale bar: 25 µm.

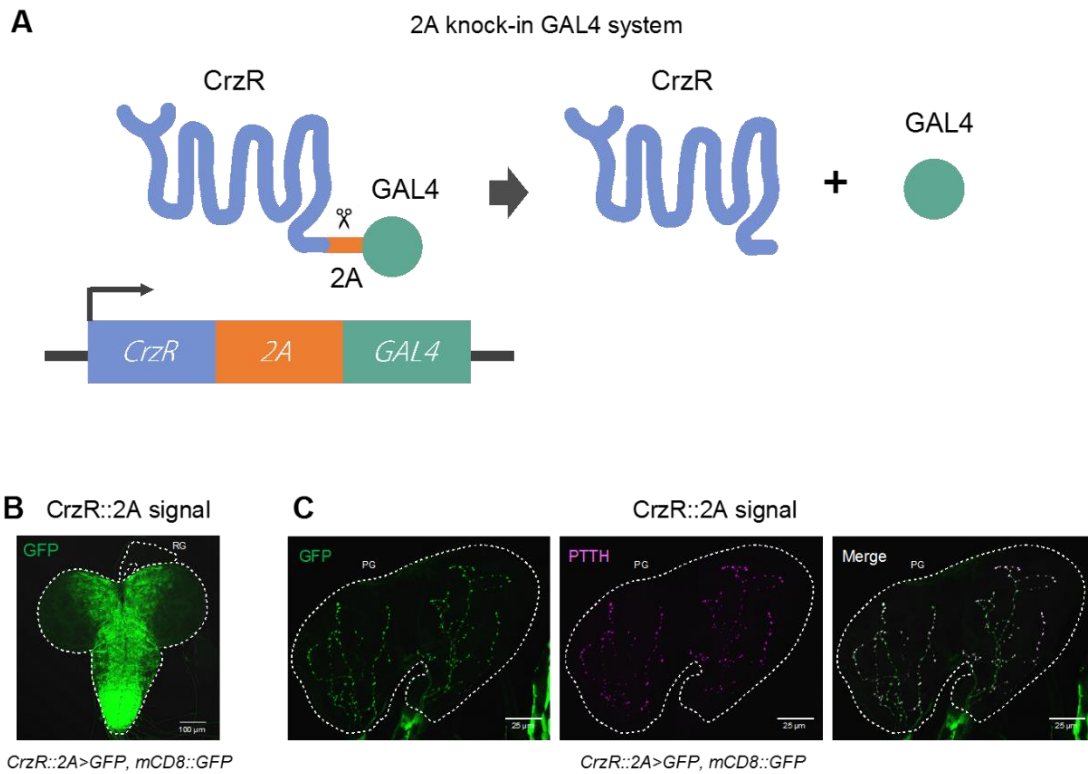


Figure 8

Visualizing *CrzR*-expressing cells using the 2A knock-in GAL4 system

(A) Schematic diagram depicting the 2A knock-in GAL4 system. A transgene containing the 2A peptide sequence and GAL4 was inserted immediately upstream of the stop codon of *CrzR*.

(B) The brain-RG complex of a *CrzR::2A>GFP, mCD8::GFP* larva in the L3 stage. Scale bar: 100 μm . (C) GFP signal reflecting *CrzR* expression was merged with PTTH signals (magenta) in the axons projecting to the PG (arrowheads). Scale bar: 25 μm .

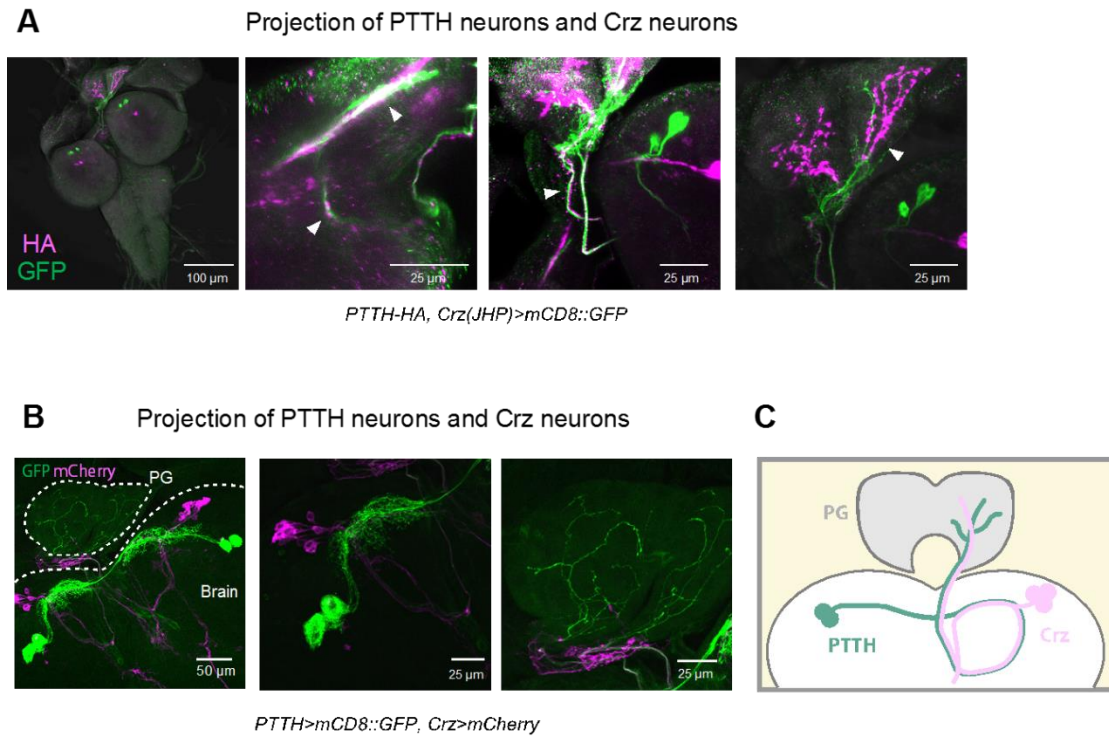
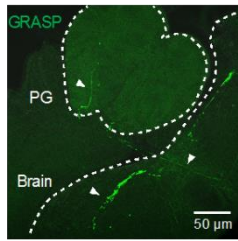


Figure 9

Crz neurons share neuronal tracts with PTTH neurons

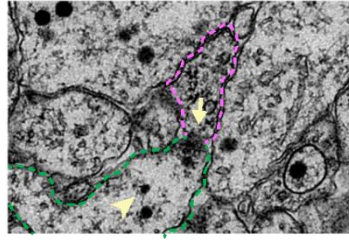
- (A) A HA tag was attached to the *ptth* promoter (magenta), and *Crz-GAL4 (JHP)* (gift from J. H. Park) drove *mCD8::GFP* (green). Both signals are merged in the neuronal tracts toward the PG (arrowheads). The axon of Crz neurons (green) are closely located near those of PTTH neurons (magenta) projecting to the PG (arrowhead). Scale bars: 100 μm and 25 μm .
- (B) *Crz-LexA* drove the expression of *mCherry* (magenta) and *PTTH-GAL4* drove the expression of *mCD8::GFP* (green). Scale bars: 50 μm and 25 μm .
- (C) Schematic diagram showing the projection of PTTH (green) and Crz neurons (pink) to the PG, only one side is represented for simplicity.

A GRASP (Crz-PTTH)



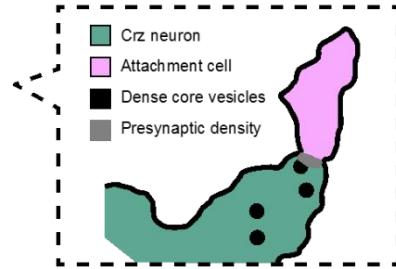
Crz>CD4::spGFP₁₁
PTTH>CD4::spGFP₁₋₁₀

B Typical synapses with DCV



Crz neuron onto PTTH neuron

C Schematic drawing of DCV fusion site



D Connectivity diagram

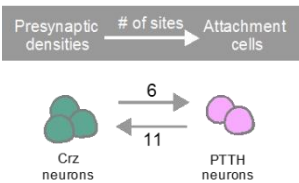


Figure 10

Investigating the connections of PTTH with Crz neurons

(A) *CD4::spGFP₁₁* was expressed by *Crz-LexA*, whereas *CD4::spGFP₁₋₁₀* was expressed by *PTTH-GAL4*. Scale bar: 50 μ m.

(B) Representative electron-microscopy micrographs of DCV fusion sites, in which Crz neurons connect to PTTH neurons. Presynaptic densities and DCVs are indicated by arrows and arrowheads, respectively. Scale bar: 500 nm.

(C) Schematic illustration of a DCV fusion site with presynaptic density (grey bar) and DCVs (black circles). Crz neurons (green) contact PG cells (pink).

(D) Connectivity diagram between PTTH and Crz neurons. Numbers describe the count of contact sites marked by presynaptic densities.

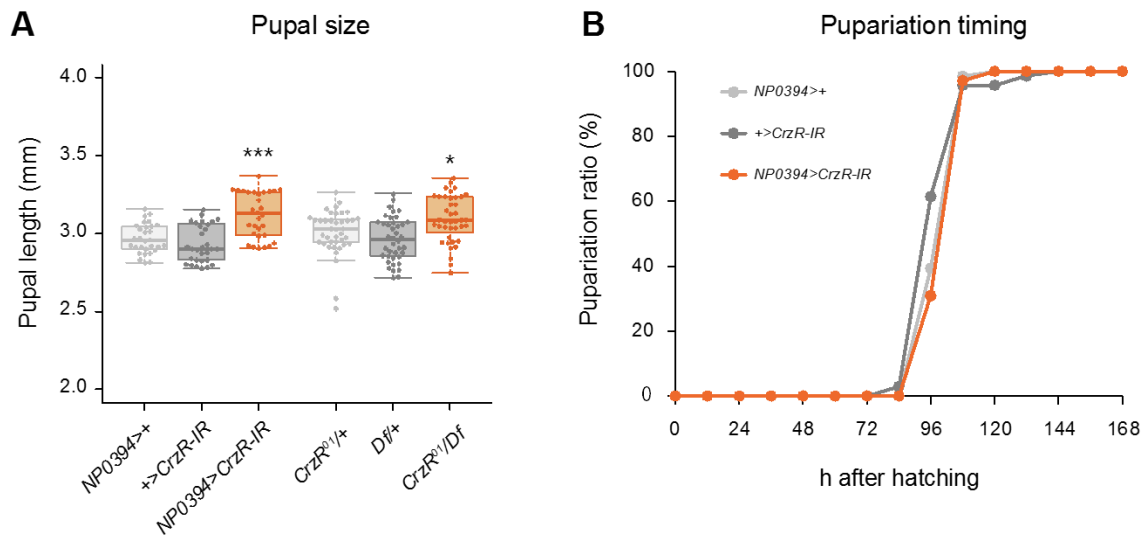
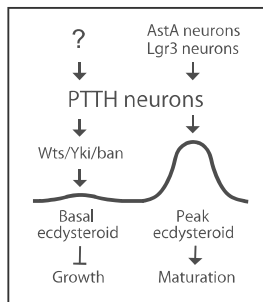


Figure 11

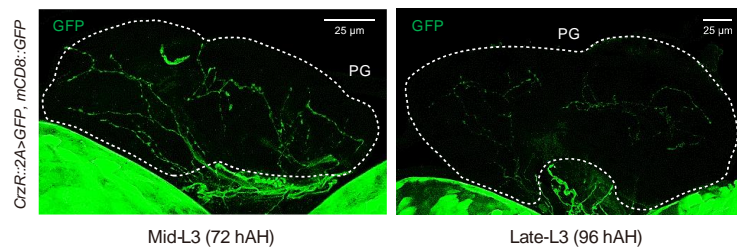
Function of *CrzR* in PTTH neurons on pupal size and pupariation timing

(A) Pupal length in control (*NP0394>+*, *+>CrzR-IR*, *CrzR⁰¹/+*, *Df/+*) and *CrzR*-deficient (*NP0394>CrzR-IR*, *CrzR⁰¹/Df*) larvae. (B) Pupariation timing of control (*NP0394>+* and *+>CrzR-IR*) and *NP0394>CrzR-RNAi* larvae. Tukey–Kramer test was used for data in panel A. *** $P \leq 0.001$, ** $P \leq 0.01$, and * $P \leq 0.05$; n.s., non-significant ($P > 0.05$).

A Role of PTTH neurons



B CrzR::2A signal



C CrzR::2A signal

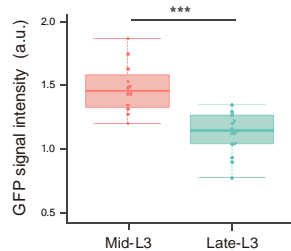


Figure 12

Changes in *CrzR* expression in PTTH neurons during the mid and late-L3 stage.

(A) Schematic diagram depicting the dual role of PTTH signaling in ecdysteroid biosynthesis. While PTTH signals affect *Wts/Yki/ban* signaling to promote basal ecdysteroid biosynthesis, they also regulate peak ecdysteroid biosynthesis, which triggers maturation. *AstA* and *Lgr3* neurons contact PTTH neurons, controlling the timing of peak ecdysteroid biosynthesis.

(B, C) *CrzR::2A* signal was stronger in the mid-L3 stage (72 hAH) than in late-L3 stage (96 hAH) larvae. (C) Quantification of GFP fluorescence intensity. hAH; hours after hatching. a.u.; arbitrary unit. Scale bar: 25 μm.

Mann–Whitney U test was used for data in panel C. *** $P \leq 0.001$, ** $P \leq 0.01$, and * $P \leq 0.05$; n.s., non-significant ($P > 0.05$).

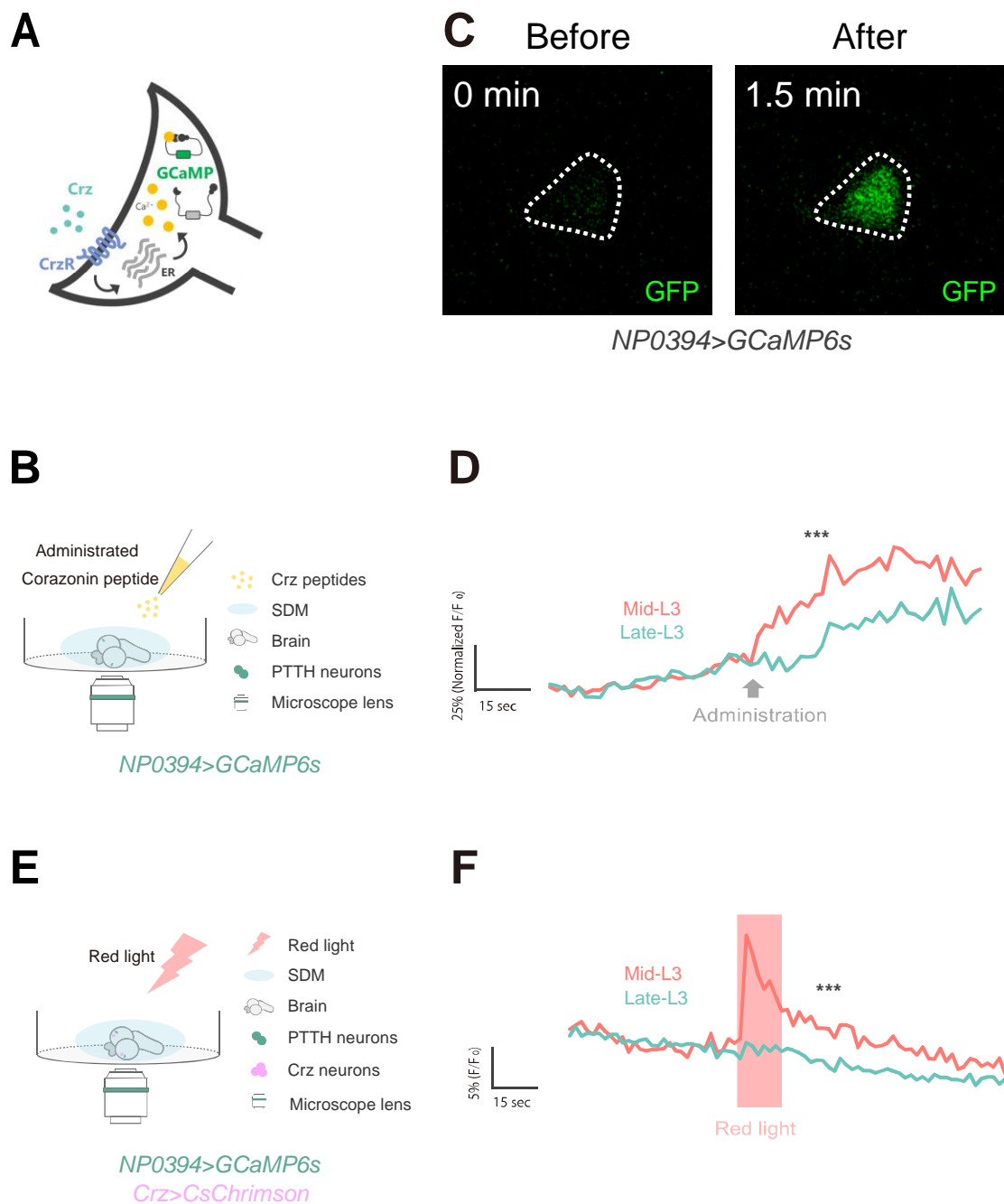


Figure 13

PTTH neurons respond to Crz peptides prominently during the mid-L3 stage

(A) Schematic illustration of CrzR causing Ca^{2+} influx. GCaMP is used to monitor the Ca^{2+} influx.

(B-F) Calcium transients in PTTH neurons in response to Crz peptide administration or CsChrimson-mediated Crz neuron activation. Brain-RG complexes were dissected from larvae expressing the calcium indicator *GCaMP6s* in PTTH neurons (*NP0394>GCaMP6s*). Samples were immersed in SDM. (C) Representative data showing that administration of Crz

peptide causes an increase in GFP intensity corresponding to calcium responses in PTTH neurons. Crz peptide was administrated at 1 min. Left panel is at 0 min; before administration of Crz peptide, right panel is at 1.5 min; after administrating Crz peptide. (E, F) *CsChrimson* was expressed in Crz neurons (*Crz>CsChrimson*). Calcium responses were detected during the mid-L3 (red) or the late-L3 (green) stage.

Kolmogorov–Smirnov test was used for data panels D and F. *** $P \leq 0.001$, ** $P \leq 0.01$, and * $P \leq 0.05$; n.s., non-significant ($P > 0.05$).

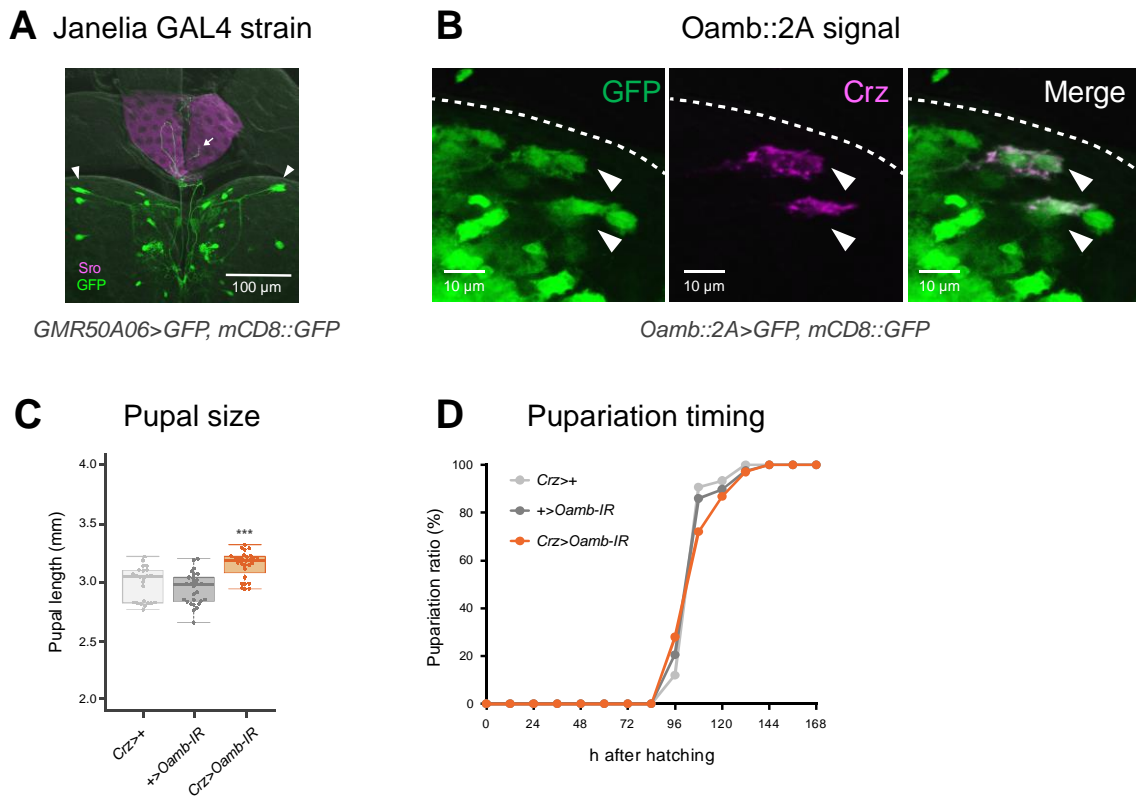


Figure 14

Oamb is expressed in Crz neurons

(A) Brain-RG complex from a late-L3 larva expressing *GFP* (green) driven by *R50A06-GAL4*. The PG was labeled with anti-Sro antibody (magenta). The cell body of Crz neurons and one axon terminus are marked by arrowheads and an arrow, respectively. Scale bar: 100 μm . (B) *Oamb::2A* signal (green) was detected in the cell body of Crz neurons (arrowheads, magenta). *GFP* and *mCD8::GFP* were driven by *Oamb::2A::GAL4*. Scale bar: 10 μm . (C) Pupal length in control (*Crz>+*, *+>Oamb-IR*) and *Crz>Oamb-RNAi* larvae. (D) Pupariation timing of control (*Crz>+* and *+>Oamb-IR*) and *Crz>Oamb-RNAi* larvae. Tukey–Kramer test was used for panel C. *** $P \leq 0.001$, ** $P \leq 0.01$, and * $P \leq 0.05$; n.s., non-significant ($P > 0.05$).

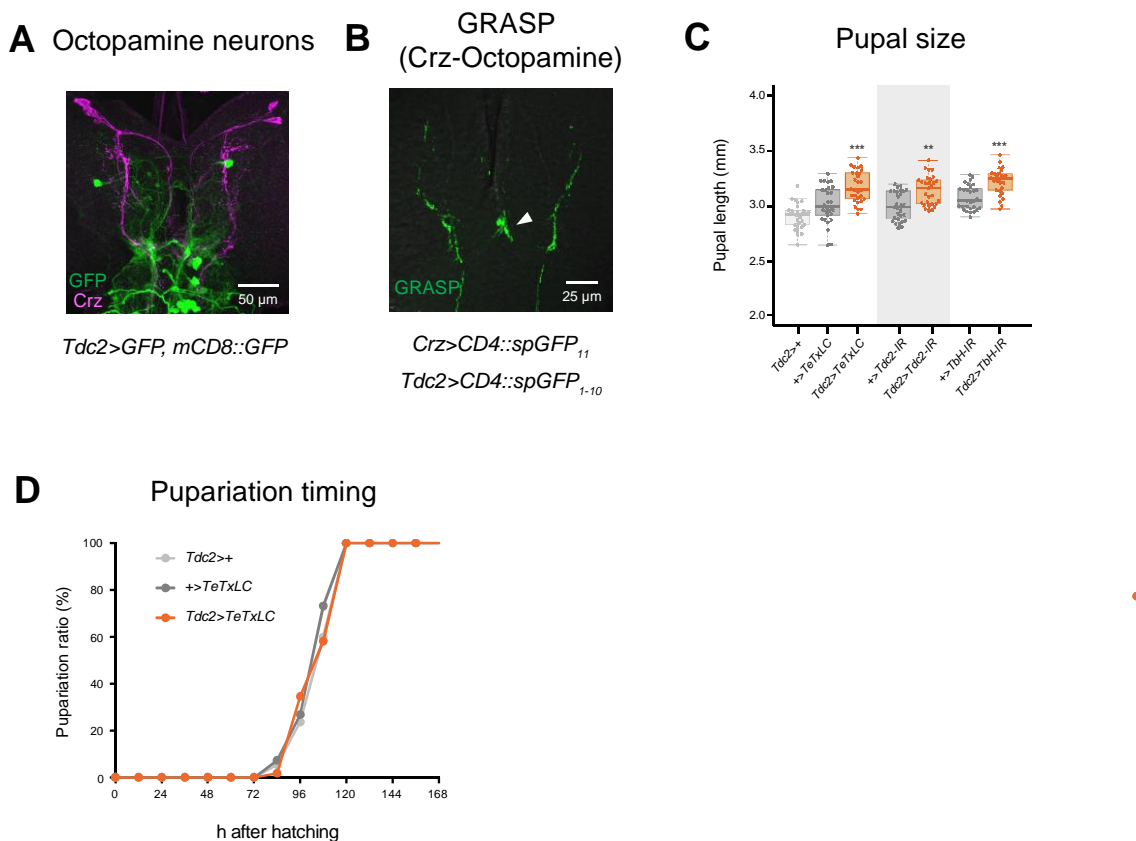


Figure 15

Octopamine neurons function upstream of Crz neurons in the regulation of systemic growth

(A) Octopamine neurons (green) were labeled with *GFP* and *mCD8::GFP* driven by *Tdc2-GAL4*. Their neurites were abundantly detected close to the dendrites of Crz neurons (magenta) in the sub-esophageal zone (SEZ). Scale bar: 50 μ m. (B) GRASP signal revealing the potential existence of synaptic connections between Crz neurons and octopamine neurons. *CD4::spGFP₁₁* was expressed by *Crz-LexA*, whereas *CD4::spGFP₁₋₁₀* was expressed by *Tdc2-GAL4*. Scale bar: 25 μ m. (C) Pupal length in control (*Tdc2>+*, *+>TeTxLC*, *+>Tdc2-IR* and *+>TbH-IR*) and *Tdc2>TeTxLC*, *Tdc2>Tdc2-IR*, *Tdc2>TbH-IR* larvae, in which octopamine neurons were inhibited. (D) Pupariation timing of control (*Tdc2>+* and *+>TeTxLC*) and *Tdc2>TeTxLC* larvae.

Tukey–Kramer test was used for panel C. *** $P \leq 0.001$, ** $P \leq 0.01$, and * $P \leq 0.05$; n.s., non-significant ($P > 0.05$).

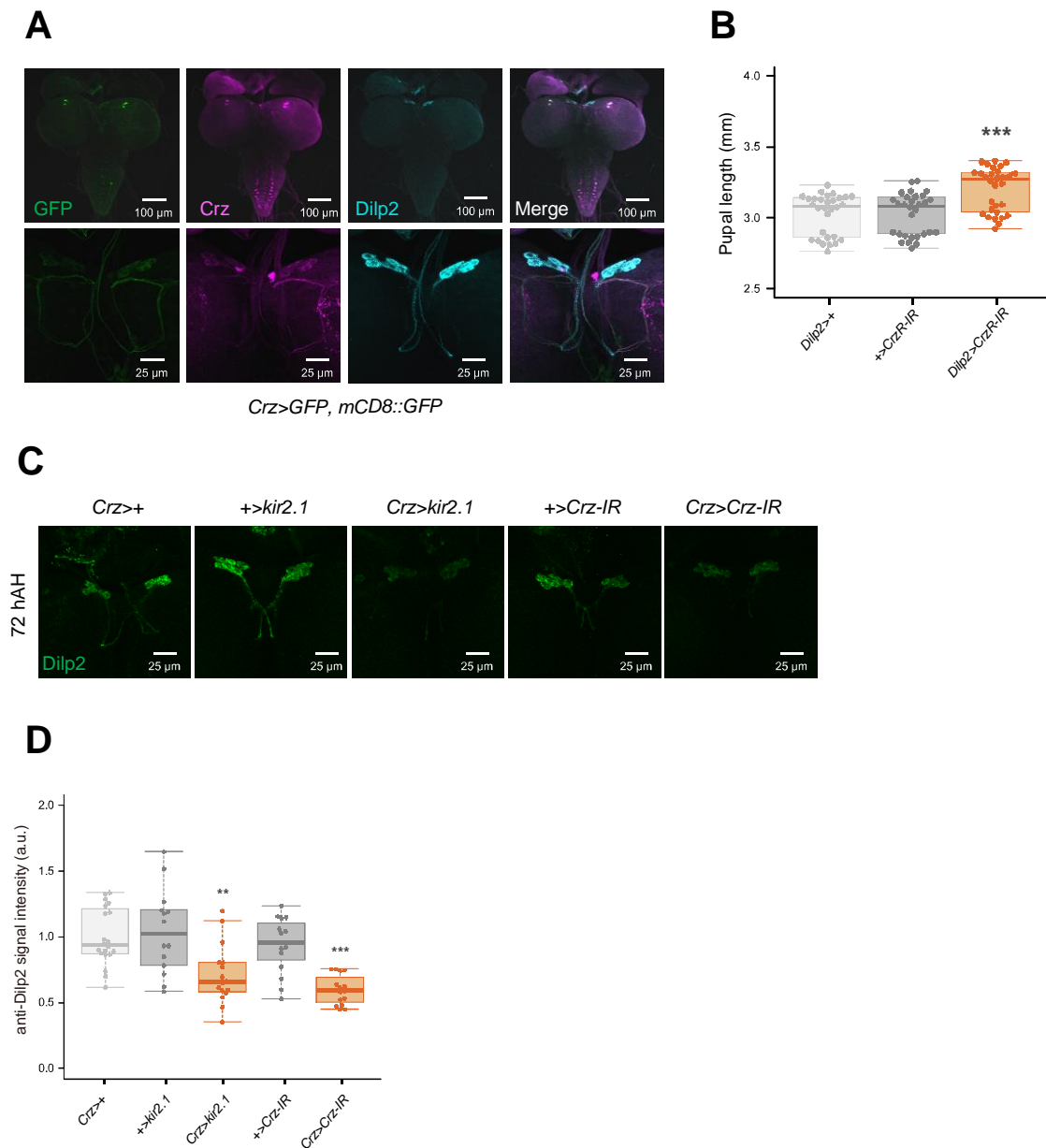


Figure 16

Crz neurons regulate Dilp2 secretion from IPCs

(A) The brain of a *Crz>GFP, mCD8::GFP* larva in the L3 stage. GFP signal reflecting Crz neurons was merged with Crz signals (magenta) and Dilp2 signals (cyan) in the brain. Scale bars: 100 μm and 25 μm .

(B) Pupal length in control (*Dilp2>+* and *+>CrzR-IR*) and *Dilp2>CrzR-IR* larvae.

(C, D) anti-Dilp2 signal was stronger in *Crz>kir2.1* and *Crz>Crz-IR* larvae than in control larvae (*Crz>*, *+>kir2.1* and *+>Crz-IR*). (D) Quantification of anti-Dilp2 fluorescence intensity in the mid-L3 stage (72 hAH). a.u.; arbitrary unit. Scale bar: 25 μm .

Tukey–Kramer test was used for panel D. *** $P \leq 0.001$, ** $P \leq 0.01$, and * $P \leq 0.05$; n.s., non-significant ($P > 0.05$).

Model

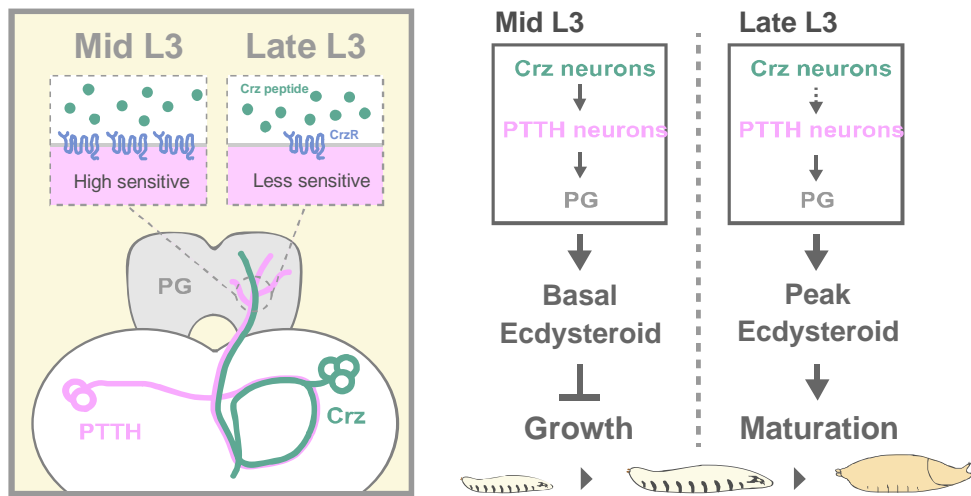


Figure 17
Crz-PTTH axis negatively regulates systemic growth by regulating basal ecdysteroid biosynthesis

Schematic representation of the Crz-PTTH neuronal axis obtained in the study. Crz neurons negatively control systemic growth by regulating basal ecdysteroid biosynthesis in the PG via PTTH neurons during the mid-L3 stage. PTTH neurons are highly sensitive to Crz peptides as *CrzR* is abundantly expressed during the mid-L3 stage. In contrast, PTTH neurons are less sensitive to Crz peptides during the late-L3 stage as *CrzR* levels decrease.

Environmental nutritional/taste cue

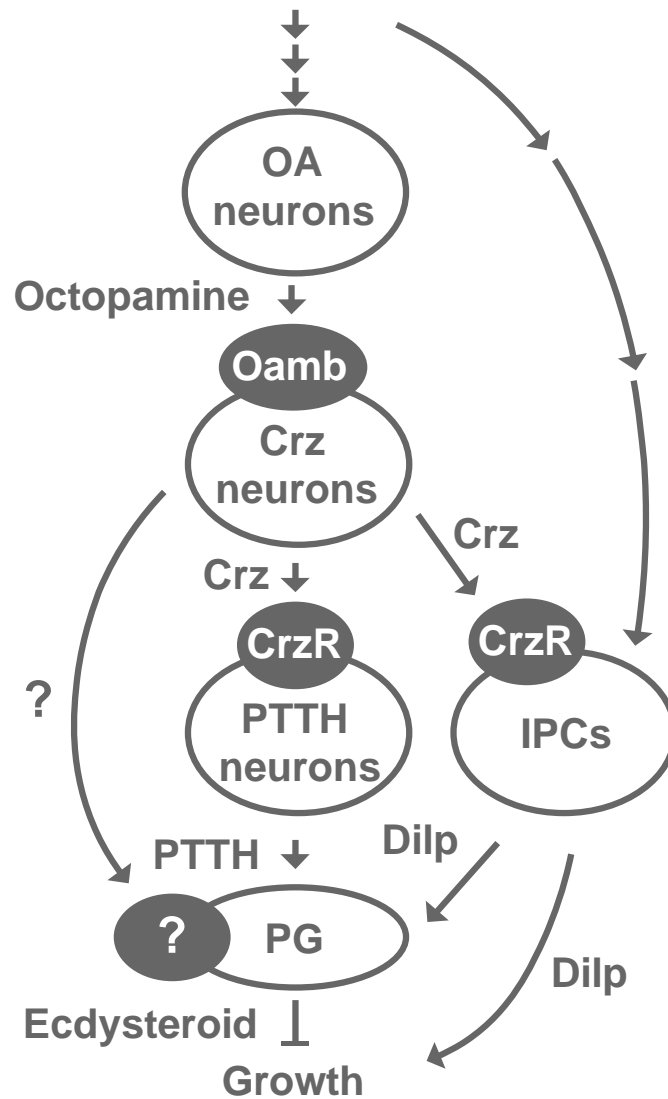


Figure 18

Crz neurons control growth both via basal ecdysteroid production and Dilp secretion

Current working model for systemic growth control by Crz neurons through regulation of ecdysteroid production in the PG and secretion of *Drosophila* insulin like peptide (Dilp) in insulin producing cells (IPCs).

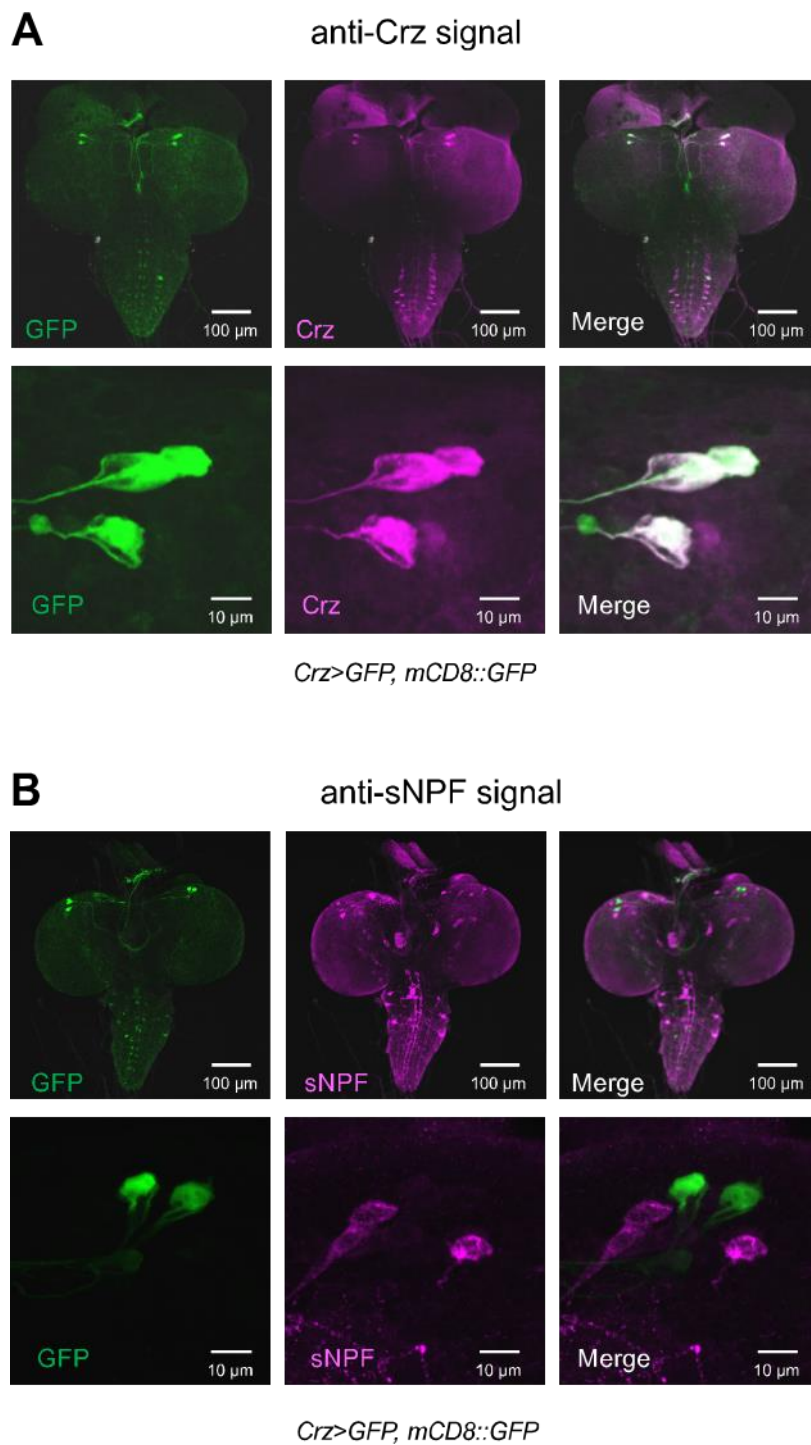


Figure 19

Three pairs of Crz neurons are distinct from sNPF neurons

(A) *Crz-GAL4* strain from Bloomington Drosophila Stock Center (#51977) is predominantly expressed in three pairs of Crz neurons in the brain. In late-L3 larvae expressing *GFP* and *mCD8::GFP* under the control of *Crz-GAL4*, the brain-RG complexes were immunostained with anti-GFP and anti-Crz antibodies. Three pairs of cell bodies were co-labeled with GFP

signals (green) and Crz signals (magenta). Scale bars: 100 μm and 10 μm .

(B) When the brain-RG complexes from *Crz>GFP, mCD8::GFP* larvae were immunostained with anti-GFP and anti-sNPF antibodies, GFP-positive Crz neurons (green) were distinct from sNPF-positive neurons (magenta), although their cell bodies were located closely to each other. Scale bars: 100 μm and 10 μm .

Vertebrates



Drosophila

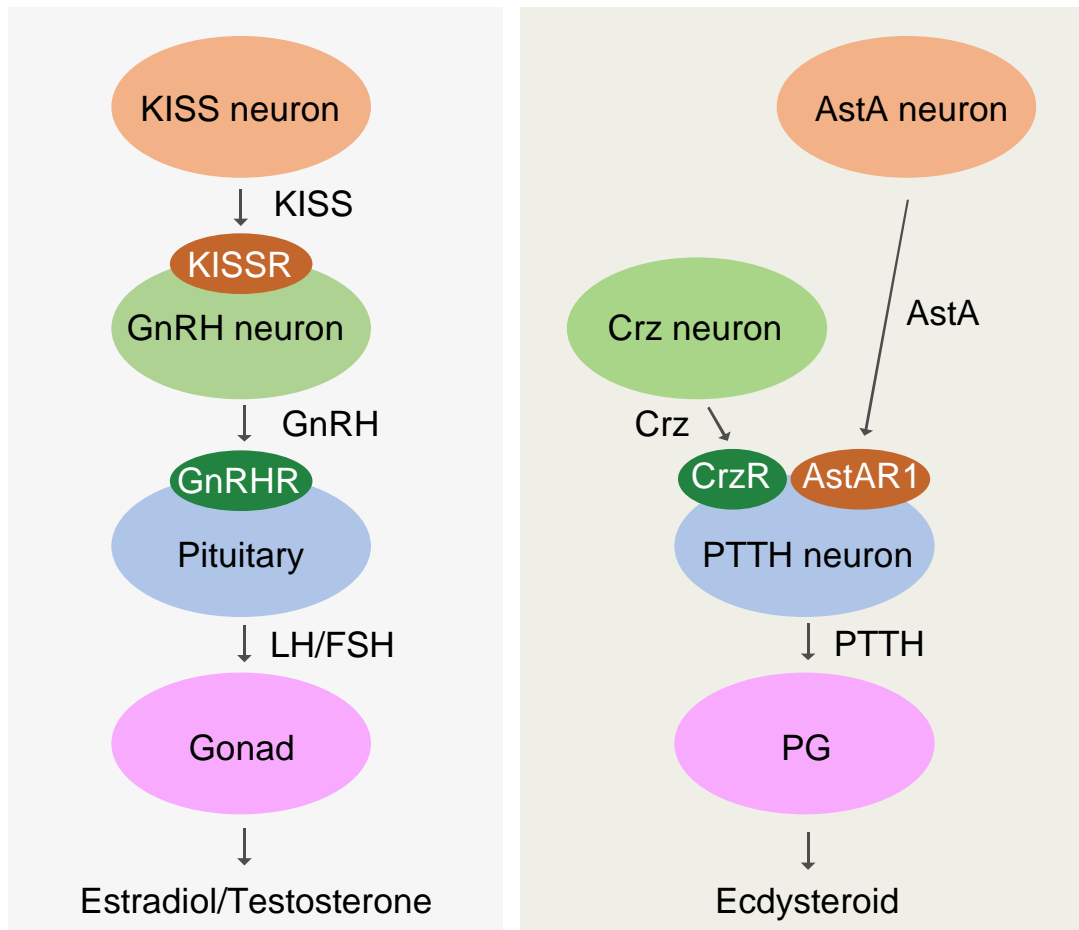


Figure 20

Evolutionarily conserved neuronal circuitry for controlling the developmental transition from the juvenile to adult stage

In vertebrates, steroid hormone biosynthesis is under the control of the hypothalamic-pituitary-gonadal (HPG) axis. In the hypothalamus, kisspeptin (KISS) acts on GnRH neurons. GnRH secretion induces the secretion of luteinizing hormone (LH) and follicle-stimulating hormone (FSH) from the pituitary gland, leading to production of estradiol and testosterone. Crz/CrzR is homologous to GnRH/GnRH receptor (GnRHR). AstA/AstA receptor (AstAR) are homologous to KISS/KISS receptor (KISSR), and control the onset of maturation via ecdysteroid production by promoting PTTH secretion.

Acknowledgements

I express my deepest gratitude to Dr. Ryusuke Niwa for mentoring me throughout my research. I am honored to work with him, Dr. Yuko Shimada-Niwa, and all other members of the Niwa lab.

I thank Dr. Yuko Shimada-Niwa, Dr. Sora Enya, Dr. Casey Schneider-Mizell, Dr. Akira Fushiki, Dr. Tom Kazimiers, and Mr. Hsin Kuang Lin for their technical support; and Ms. Reiko Kise for her technical assistance.

For fruitful collaboration, I thank Dr. Takashi Nishimura for performing LC/MS-MS; Dr. Shu Kondo for generating and proving 2A knock-in GAL4 and CRISPR/Cas9 mutant; Dr. Hiromu Tanimoto for generating and proving 2A knock-in GAL4; Dr. Yuya Ohhara for generating and proving Crz-LexA; Mr. Sebastian Hückesfeld, Dr. Philipp Schlegel, Dr. Michael J Pankratz, and Dr. Albert Cardona for supporting and performing connectome analysis.

I thank Dr. Hubert Amrein, Dr. Yoshi Aso, Dr. Barry Dickson, Dr. Yoshiki Hayashi, Dr. Young-Joon Kim, Dr. Satoru Kobayashi, Dr. Pierre Leopold, Mr. Todd Laverty, Dr. Li Y. McCurdy, Dr. Ryo Minegishi, Dr. Michael B. O'Connor, Dr. Jae H. Park, Dr. Kim F. Rewitz, Dr. Nuria Romero, Dr. Paul H. Taghert, Dr. Jan A. Veenstra, Dr. Naoki Yamanaka, Dr. Kweon Yu, Dr. Christian Wegener, Dr. Shigeo Hayashi, the Bloomington *Drosophila* Stock Center, the *Drosophila* Genetics Resource Center, the Janelia Research Campus, the National Institute of Genetics, and the Vienna *Drosophila* RNAi Center for providing *Drosophila* stocks and reagents.

I thank Kagayaki Kato, Dr. Megha, Dr. Naoki Okamoto, Dr. Ryunosuke Minami, Dr. Shigeaki Yoshiura, Dr. Tadashi Uemura, and Dr. Takashi Suzuki for giving me valuable feedbacks.

I thank Dr. Ryusuke Niwa, Dr. Satoru Kobayashi, Dr. Chikafumi Chiba, and Dr. Tetsuo Hashimoto for my dissertation advisory committee.

This work was supported by a grant of the Japan Society for the Promotion of Science (JSPS).

References

1. Miller, W.L., and Auchus, R.J. (2011). The Molecular Biology, Biochemistry, and Physiology of Human Steroidogenesis and Its Disorders. *Endocrine Reviews* 32, 81–151.
2. Danielsen, E.T., Moeller, M.E., Dorry, E., Komura-Kawa, T., Fujimoto, Y., Troelsen, J.T., Herder, R., O'Connor, M.B., Niwa, R., and Rewitz, K.F. (2014). Transcriptional control of steroid biosynthesis genes in the *Drosophila* prothoracic gland by Ventral veins lacking and Knirps. *PLoS Genetics* 10, e1004343.
3. Imura, E., Shimada-Niwa, Y., and Niwa, R. (2016). 環境に応じて昆虫の発育を司るステロイドホルモンの生合成調節メカニズム. *生物科学* 67, 177–183.
4. Niwa, R., and Niwa, Y.S. (2014). Enzymes for ecdysteroid biosynthesis: their biological functions in insects and beyond. *Bioscience, Biotechnology, and Biochemistry* 78, 1283–1292.
5. Gilbert, L.I., Rybczynski, R., and Warren, J.T. (2002). Control and biochemical nature of the ecdysteroidogenic pathway. *Annual Review of Entomology* 47, 883–916.
6. Moeller, M.E., Danielsen, E.T., Herder, R., O'Connor, M.B., and Rewitz, K.F. (2013). Dynamic feedback circuits function as a switch for shaping a maturation-inducing steroid pulse in *Drosophila*. *Development* 140, 4730–4739.
7. Boulan, L., Milán, M., and Léopold, P. (2015). The Systemic Control of Growth. *Cold Spring Harbor perspectives in biology* 7, a019117.
8. Colombani, J., Bianchini, L., Layalle, S., Pondeville, E., Dauphin-Villemant, C., Antoniewski, C., Carré, C., Noselli, S., and Léopold, P. (2005). Antagonistic Actions of Ecdysone and Insulins Determine Final Size in *Drosophila*. *Science* 310, 667–670.
9. Delanoue, R., Slaidina, M., and Léopold, P. (2010). The Steroid Hormone Ecdysone Controls Systemic Growth by Repressing dMyc Function in *Drosophila* Fat Cells. *Developmental Cell* 18, 1012–1021.
10. Rewitz, K.F., Yamanaka, N., and O'Connor, M.B. (2013). Developmental checkpoints and feedback circuits time insect maturation. *Current topics in developmental biology* 103, 1–33.
11. Boulan, L., Martín, D., and Milán, M. (2013). bantam miRNA promotes systemic growth by connecting insulin signaling and ecdysone production. *Current biology : CB* 23, 473–478.
12. Moeller, M.E., Nagy, S., Gerlach, S.U., Soegaard, K.C., Danielsen, E.T., Texada, M.J., and Rewitz, K.F. (2017). Warts Signaling Controls Organ and Body Growth through Regulation of Ecdysone. *Current Biology* 27, 1652-1659.e4.
13. Niwa, Y.S., and Niwa, R. (2014). Neural control of steroid hormone biosynthesis during development in the fruit fly *Drosophila melanogaster*. *Genes & Genetic Systems* 89, 27–34.
14. Yamanaka, N., Rewitz, K.F., and O'Connor, M.B. (2013). Ecdysone control of developmental transitions: lessons from *Drosophila* research. *Annual Review of Entomology* 58, 497–516.
15. Siegmund, T., and Korge, G. (2001). Innervation of the ring gland of *Drosophila melanogaster*. *Journal of Comparative Neurology* 431, 481–491.
16. McBrayer, Z., Ono, H., Shimell, M., Parvy, J.-P., Beckstead, R.B., Warren, J.T., Thummel, C.S., Dauphin-Villemant, C., Gilbert, L.I., and O'Connor, M.B. (2007). Prothoracicotropic hormone regulates developmental timing and body size in *Drosophila*. *Developmental cell* 13, 857–71.
17. Shimada-Niwa, Y., and Niwa, R. (2014). Serotonergic neurons respond to nutrients and regulate the timing of steroid hormone biosynthesis in *Drosophila*. *Nature Communications* 5, 5778.
18. Yokoyama, T. (1956). The morphology and innervation of the prothoracic gland in the silkworm, *Bombyx mori*. *J. Sericult. Sci. Jpn.* 25, 87–94.
19. Yamanaka, N., Zitnan, D., Kim, Y.-J., Adams, M.E., Hua, Y.-J., Suzuki, Y., Suzuki, M., Suzuki, A., Satake, H., Mizoguchi, A., *et al.* (2006). Regulation of insect steroid hormone

- biosynthesis by innervating peptidergic neurons. *Proceedings of the National Academy of Sciences of the United States of America* *103*, 8622–7.
20. Okajima, A., Kumagai, K., and Watanabe, N. (1989). The involvement of interoceptive chemosensory activity in the nervous regulation of the prothoracic gland in a moth, *Mamestra brassicae*. *Zoological Science* *6*, p859-866.
 21. Richter, K., and Böhm, G.-A. (1997). The molting gland of the cockroach *Periplaneta americana*: secretory activity and its regulation. *General Pharmacology: The Vascular System* *29*, 17–21.
 22. Pfeiffer, B.D., Jenett, A., Hammonds, A.S., Ngo, T.-T.B., Misra, S., Murphy, C., Scully, A., Carlson, J.W., Wan, K.H., Lavery, T.R., *et al.* (2008). Tools for neuroanatomy and neurogenetics in *Drosophila*. *Proceedings of the National Academy of Sciences of the United States of America* *105*, 9715–9720.
 23. Jenett, A., Rubin, G.M., Ngo, T.-T.B., Shepherd, D., Murphy, C., Dionne, H., Pfeiffer, B.D., Cavallaro, A., Hall, D., Jeter, J., *et al.* (2012). A GAL4-Driver Line Resource for *Drosophila* Neurobiology. *Cell Reports* *2*, 991–1001.
 24. Li, H.-H., Kroll, J.R., Lennox, S.M., Ogundeyi, O., Jeter, J., Depasquale, G., and Truman, J.W. (2014). A GAL4 driver resource for developmental and behavioral studies on the larval CNS of *Drosophila*. *Cell Reports* *8*, 897–908.
 25. Struhl, G., and Basler, K. (1993). Organizing activity of wingless protein in *Drosophila*. *Cell* *72*, 527–540.
 26. Germani, F., Bergantinos, C., and Johnston, L.A. (2018). Mosaic analysis in *drosophila*. *Genetics* *208*, 473–490.
 27. Park, D., Veenstra, J.A., Park, J.H., and Taghert, P.H. (2008). Mapping Peptidergic Cells in *Drosophila*: Where DIMM Fits In. *PLoS ONE* *3*, e1896.
 28. Predel, R., Neupert, S., Russell, W.K., and Scheibner, O. (2007). Corazonin in insects. *Peptides* *28*, 3–10.
 29. Choi, Y.J., Lee, G., Hall, J.C., and Park, J.H. (2005). Comparative analysis of Corazonin-encoding genes (Crz's) in *Drosophila* species and functional insights into Crz-expressing neurons. *The Journal of comparative neurology* *482*, 372–385.
 30. Saalfeld, S., Cardona, A., Hartenstein, V., and Tomancak, P. (2009). CATMAID: collaborative annotation toolkit for massive amounts of image data. *Bioinformatics* *25*, 1984–1986.
 31. Schneider-Mizell, C.M., Gerhard, S., Longair, M., Kazimiers, T., Li, F., Zwart, M.F., Champion, A., Midgley, F.M., Fetter, R.D., Saalfeld, S., *et al.* (2016). Quantitative neuroanatomy for connectomics in *Drosophila*. *eLife* *5*.
 32. Gerhard, S., Andrade, I., Fetter, R.D., Cardona, A., and Schneider-Mizell, C.M. (2017). Conserved neural circuit structure across *Drosophila* larval development revealed by comparative connectomics. *eLife* *6*.
 33. van den Pol, A.N. (2012). Neuropeptide Transmission in Brain Circuits. *Neuron* *76*, 98–115.
 34. Schlegel, P., Texada, M.J., Miroschnikow, A., Schoofs, A., Hückesfeld, S., Peters, M., Schneider-Mizell, C.M., Lacin, H., Li, F., Fetter, R.D., *et al.* (2016). Synaptic transmission parallels neuromodulation in a central food-intake circuit. *eLife* *5*.
 35. Tayler, T.D., Pacheco, D.A., Hergarden, A.C., Murthy, M., and Anderson, D.J. (2012). A neuropeptide circuit that coordinates sperm transfer and copulation duration in *Drosophila*. *Proceedings of the National Academy of Sciences of the United States of America* *109*, 20697–20702.
 36. Baines, R.A., Uhler, J.P., Thompson, A., Sweeney, S.T., and Bate, M. (2001). Altered electrical properties in *Drosophila* neurons developing without synaptic transmission. *The Journal of neuroscience* *21*, 1523–1531.
 37. Paradis, S., Sweeney, S.T., and Davis, G.W. (2001). Homeostatic Control of Presynaptic Release Is Triggered by Postsynaptic Membrane Depolarization. *Neuron* *30*, 737–749.

38. Lavrynenko, O., Rodenfels, J., Carvalho, M., Dye, N.A., Lafont, R., Eaton, S., and Shevchenko, A. (2015). The ecdysteroidome of *Drosophila*: influence of diet and development. *Development* *142*, 3758–3768.
39. Blais, C., Blasco, T., Maria, A., Dauphin-Villemant, C., and Lafont, R. (2010). Characterization of ecdysteroids in *Drosophila melanogaster* by enzyme immunoassay and nano-liquid chromatography–tandem mass spectrometry. *Journal of Chromatography B* *878*, 925–932.
40. Hikiba, J., Ogihara, M.H., Iga, M., Saito, K., Fujimoto, Y., Suzuki, M., and Kataoka, H. (2013). Simultaneous quantification of individual intermediate steroids in silkworm ecdysone biosynthesis by liquid chromatography–tandem mass spectrometry with multiple reaction monitoring. *Journal of Chromatography B* *915–916*, 52–56.
41. Li, Y., Warren, J.T., Boysen, G., Gilbert, L.I., Gold, A., Sangaiah, R., Ball, L.M., and Swenberg, J.A. (2006). Profiling of ecdysteroids in complex biological samples using liquid chromatography/ion trap mass spectrometry. *Rapid Communications in Mass Spectrometry* *20*, 185–192.
42. Miyashita, M., Matsushita, K., Nakamura, S., Akahane, S., Nakagawa, Y., and Miyagawa, H. (2011). LC/MS/MS identification of 20-hydroxyecdysone in a scorpion (*Liocheles australasiae*) and its binding affinity to in vitro-translated molting hormone receptors. *Insect Biochemistry and Molecular Biology* *41*, 932–937.
43. Diao, F., and White, B.H. (2012). A novel approach for directing transgene expression in *Drosophila*: T2A-Gal4 in-frame fusion. *Genetics* *190*, 1139–1144.
44. Colombani, J., Andersen, D.S., Boulan, L., Boone, E., Romero, N., Virolle, V., Texada, M., and Léopold, P. (2015). *Drosophila* Lgr3 Couples Organ Growth with Maturation and Ensures Developmental Stability. *Current Biology* *25*, 2723–2729.
45. Devעי, D., Martin, F.A., Leopold, P., and Romero, N.M. (2019). AstA Signaling Functions as an Evolutionary Conserved Mechanism Timing Juvenile to Adult Transition. *Current Biology* *29*, 813-822.e4.
46. Vallejo, D.M., Juarez-Carreño, S., Bolivar, J., Morante, J., and Dominguez, M. (2015). A brain circuit that synchronizes growth and maturation revealed through Dilp8 binding to Lgr3. *Science* *350*, aac6767.
47. Garelli, A., Heredia, F., Casimiro, A.P., Macedo, A., Nunes, C., Garcez, M., Dias, A.R.M., Volonte, Y.A., Uhlmann, T., Caparros, E., *et al.* (2015). Dilp8 requires the neuronal relaxin receptor Lgr3 to couple growth to developmental timing. *Nature Communications* *6*, 8732.
48. Jaszczak, J.S., Wolpe, J.B., Bhandari, R., Jaszczak, R.G., and Halme, A. (2016). Growth Coordination During *Drosophila melanogaster* Imaginal Disc Regeneration Is Mediated by Signaling Through the Relaxin Receptor Lgr3 in the Prothoracic Gland. *Genetics*, genetics.116.193706.
49. Pan, X., and O'Connor, M.B. (2019). Developmental Maturation: *Drosophila* AstA Signaling Provides a Kiss to Grow Up. *Current biology : CB* *29*, R161–R164.
50. Chen, T.-W., Wardill, T.J., Sun, Y., Pulver, S.R., Renninger, S.L., Baohan, A., Schreiter, E.R., Kerr, R.A., Orger, M.B., Jayaraman, V., *et al.* (2013). Ultrasensitive fluorescent proteins for imaging neuronal activity. *Nature* *499*, 295–300.
51. Roch, G.J., Busby, E.R., and Sherwood, N.M. (2011). Evolution of GnRH: Diving deeper. *General and Comparative Endocrinology* *171*, 1–16.
52. Hou, Q.L., Jiang, H.B., Gui, S.H., Chen, E.H., Wei, D.D., Li, H.M., Wang, J.J., and Smagghe, G. (2017). A role of corazonin receptor in larval-pupal transition and pupariation in the oriental fruit fly *Bactrocera dorsalis* (Hendel) (Diptera: Tephritidae). *Frontiers in Physiology* *8*, 77.
53. Klapoetke, N.C., Murata, Y., Kim, S.S., Pulver, S.R., Birdsey-Benson, A., Cho, Y.K., Morimoto, T.K., Chuong, A.S., Carpenter, E.J., Tian, Z., *et al.* (2014). Independent optical excitation of distinct neural populations. *Nature Methods* *11*, 338.

54. Han, K.A., Millar, N.S., and Davis, R.L. (1998). A novel octopamine receptor with preferential expression in *Drosophila* mushroom bodies. *The Journal of neuroscience* *18*, 3650–3658.
55. Roeder, T. (1999). Octopamine in invertebrates. *Progress in Neurobiology* *59*, 533–561.
56. Roeder, T. (2005). Tyramine and octopamine: ruling behavior and metabolism. *Annual Review of Entomology* *50*, 447–477.
57. Verlinden, H., Vleugels, R., Marchal, E., Badisco, L., Pflüger, H.J., Blenau, W., and Broeck, J. Vanden (2010). The role of octopamine in locusts and other arthropods. *Journal of Insect Physiology* *56*, 854–867.
58. Cole, S.H., Carney, G.E., McClung, C.A., Willard, S.S., Taylor, B.J., and Hirsh, J. (2005). Two Functional but Noncomplementing *Drosophila* Tyrosine Decarboxylase Genes. *Journal of Biological Chemistry* *280*, 14948–14955.
59. Kendroud, S., Bohra, A.A., Kuert, P.A., Nguyen, B., Guillermin, O., Sprecher, S.G., Reichert, H., VijayRaghavan, K., and Hartenstein, V. (2018). Structure and development of the subesophageal zone of the *Drosophila* brain. II. Sensory compartments. *Journal of Comparative Neurology* *526*, 33–58.
60. Monastirioti, M., Linn, C.E., and White, K. (1996). Characterization of *Drosophila* tyramine beta-hydroxylase gene and isolation of mutant flies lacking octopamine. *The Journal of neuroscience* *16*, 3900–3911.
61. Danielsen, E.T., Moeller, M.E., and Rewitz, K.F. (2013). Nutrient signaling and developmental timing of maturation. *Current topics in developmental biology* *105*, 37–67.
62. Agrawal, N., Delanoue, R., Mauri, A., Basco, D., Pasco, M., Thorens, B., and Léopold, P. (2016). The *Drosophila* TNF Eiger Is an Adipokine that Acts on Insulin-Producing Cells to Mediate Nutrient Response. *Cell Metabolism* *23*, 675–684.
63. Colombani, J., Raisin, S., Pantalacci, S., Radimerski, T., Montagne, J., and Léopold, P. (2003). A Nutrient Sensor Mechanism Controls *Drosophila* Growth. *Cell* *114*, 739–749.
64. Delanoue, R., Meschi, E., Agrawal, N., Mauri, A., Tsatskis, Y., McNeill, H., and Léopold, P. (2016). *Drosophila* insulin release is triggered by adipose Stunted ligand to brain Methuselah receptor. *Science* *353*, 1553–1556.
65. Koyama, T., and Mirth, C.K. (2016). Growth-Blocking Peptides As Nutrition-Sensitive Signals for Insulin Secretion and Body Size Regulation. *PLOS Biology* *14*, e1002392.
66. Rajan, A., and Perrimon, N. (2012). *Drosophila* Cytokine Unpaired 2 Regulates Physiological Homeostasis by Remotely Controlling Insulin Secretion. *Cell* *151*, 123–137.
67. Sano, H., Nakamura, A., Texada, M.J., Truman, J.W., Ishimoto, H., Kamikouchi, A., Nibu, Y., Kume, K., Ida, T., and Kojima, M. (2015). The Nutrient-Responsive Hormone CCHamide-2 Controls Growth by Regulating Insulin-like Peptides in the Brain of *Drosophila melanogaster*. *PLOS Genetics* *11*, e1005209.
68. Singh, R.N. (1997). Neurobiology of the gustatory systems of *Drosophila* and some terrestrial insects. *Microscopy research and technique* *39*, 547–63.
69. Megha, Wegener, C., and Hasan, G. (2019). ER-Ca²⁺ sensor STIM regulates neuropeptides required for development under nutrient restriction in *Drosophila*. *PLOS ONE* *14*, e0219719.
70. Nässel, D.R., Enell, L.E., Santos, J.G., Wegener, C., and Johard, H.A.D. (2008). A large population of diverse neurons in the *Drosophila* central nervous system expresses short neuropeptide F, suggesting multiple distributed peptide functions. *BMC neuroscience* *9*, 90.
71. Ellison, P.T., Reiches, M.W., Shattuck-Faegre, H., Breakey, A., Konecna, M., Urlacher, S., and Wobber, V. (2012). Puberty as a life history transition. *Annals of Human Biology* *39*, 352–360.
72. Plant, T.M. (2015). Neuroendocrine control of the onset of puberty. *Frontiers in Neuroendocrinology* *38*, 73–88.
73. Navarro, V.M., and Tena-Sempere, M. (2012). Neuroendocrine control by kisspeptins: role in metabolic regulation of fertility. *Nature Reviews Endocrinology* *8*, 40–53.

74. Pinilla, L., Aguilar, E., Dieguez, C., Millar, R.P., and Tena-Sempere, M. (2012). Kisspeptins and Reproduction: Physiological Roles and Regulatory Mechanisms. *Physiological Reviews* 92, 1235–1316.
75. Roa, J., Aguilar, E., Dieguez, C., Pinilla, L., and Tena-Sempere, M. (2008). New frontiers in kisspeptin/GPR54 physiology as fundamental gatekeepers of reproductive function. *Frontiers in Neuroendocrinology* 29, 48–69.
76. Tena-Sempere, M. (2008). Timeline: the role of kisspeptins in reproductive biology. *Nature Medicine* 14, 1196–1196.
77. Herbison, A.E. (2016). Control of puberty onset and fertility by gonadotropin-releasing hormone neurons. *Nature Reviews Endocrinology* 12, 452–466.
78. Ojeda, S.R., and Skinner, M.K. (2006). Puberty in the Rat. *Knobil and Neill's Physiology of Reproduction* 2, 2061–2126.
79. Zandawala, M., Tian, S., and Elphick, M.R. (2018). The evolution and nomenclature of GnRH-type and corazonin-type neuropeptide signaling systems. *General and Comparative Endocrinology* 264, 64–77.
80. Rulifson, E.J., Kim, S.K., and Nusse, R. (2002). Ablation of insulin-producing neurons in flies: Growth and diabetic phenotypes. *Science* 296, 1118–1120.
81. Ito, K., Suzuki, K., Estes, P., Ramaswami, M., Yamamoto, D., and Strausfeld, N.J. (1998). The organization of extrinsic neurons and their implications in the functional roles of the mushroom bodies in *Drosophila melanogaster* Meigen. *Learning & memory* 5, 52–77.
82. Sha, K., Choi, S.-H., Im, J., Lee, G.G., Loeffler, F., and Park, J.H. (2014). Regulation of Ethanol-Related Behavior and Ethanol Metabolism by the Corazonin Neurons and Corazonin Receptor in *Drosophila melanogaster*. *PLoS ONE* 9, e87062.
83. Imura, E., Yoshinari, Y., Shimada-Niwa, Y., and Niwa, R. (2017). Protocols for visualizing steroidogenic organs and their interactive organs with immunostaining in the fruit fly *drosophila melanogaster*. *Journal of Visualized Experiments*, e55519.
84. Veenstra, J.A. (1991). Presence of corazonin in three insect species, and isolation and identification of [His7]corazonin from *Schistocerca americana*. *Peptides* 12, 1285–1289.
85. Yamanaka, N., Romero, N.M., Martin, F.A., Rewitz, K.F., Sun, M., O'Connor, M.B., and Léopold, P. (2013). Neuroendocrine control of *Drosophila* larval light preference. *Science* 341, 1113–1116.
86. Ohyama, T., Schneider-Mizell, C.M., Fetter, R.D., Aleman, J.V., Franconville, R., Rivera-Alba, M., Mense, B.D., Branson, K.M., Simpson, J.H., Truman, J.W., *et al.* (2015). A multilevel multimodal circuit enhances action selection in *Drosophila*. *Nature* 520, 633–639.
87. Saalfeld, S., Cardona, A., Hartenstein, V., and Tomancak, P. (2009). CATMAID: collaborative annotation toolkit for massive amounts of image data. *Bioinformatics* 25, 1984–1986.
88. Abramoff, M.D., Magalhães, P.J., and Ram, S.J. (2004). Image Processing with ImageJ. *Biophotonics Int.* 11, 36–42.